FCP Report No. 9

CYCLIC STRESS-STRAIN BEHAVIOR AND FATIGUE RESISTANCE OF TWO STRUCTURAL STEELS

by

J. F. Martin
Department of Theoretical and Applied Mechanics

ABSTRACT

The stress-strain behavior and fatigue resistance of two structural steels are investigated. Specimens were cut from thin steel sheets and cylindrical steel bars. The thin sheet specimens were designed so as to prevent buckling. Total axial strain for these sheet specimens was computed from the transverse strain and load by an analytical expression programmed through an analog computer. The monotonic and stable cyclic stress-strain properties for both steels are similar. Cycle dependent hardening and softening were not as evident for the sheet steel. Three different procedures for determining the stable cyclic behavior produced considerably different results. Strain-life data showed the effects of a single initial overstrain and periodic overstrains. Both types of overstraining of the bar steel produced similar fatigue data to that of the non-overstrained and initially overstrained sheet steel results.

A Report of the
FRACTURE CONTROL PROGRAM

College of Engineering, University of Illinois
Urbana, Illinois 61801
October, 1973

INTRODUCTION

In step with the increasing necessity to prevent fatigue failures in structural components, new procedures continually appear that more closely account for the actual causes of fatigue damage. These analyses are obtained by basing failure predictions on the behavior of the metal at the highly strained region where cracks initiate (1-8)*. Figure 1 shows the concept behind this approach. Any procedure of this type assumes that the necessary data to perform a fatigue analysis can be generated by laboratory specimens. As part of the Fracture Control Program at the University of Illinois, a fatigue damage analysis of an automotive fan blade was made. The procedure (9) modeled the uniaxial cyclic behavior of the fan blade material, and utilized this model in a mechanics analysis to calculate the stress-strain response at the highly strained zone. From the stresses and strains at the critical location, a cumulative damage procedure based on uniaxial fatigue data predicted the number of reversals for crack initiation.

This report presents the stress-strain and fatigue properties (2, 4, 10-15) of the fan blade metal. Because of the thin specimens machined from the sheet metal, various specimen designs and testing techniques were used in attempts to prevent cyclic buckling.

Behavior of another structural steel, supplied in round bars, was compared with the sheet steel. This bar steel is a common type, the properties of which might exist in a "data bank". Similarity in the properties of these two steels are determined.

---

*Numbers in parentheses refer to references.

COMPOSITION OF METALS*

Although both metals can be classified as structural steels, their compositions are quite different. One steel was in the form of a thin (0.070 inch thick) sheet. This sheet was removed from the assembly process just prior to the forming operation for the fan blade. The other steel was supplied in the form of round 3/4 inch diameter bar stock. Table 1 lists the composition of both steels. Hardness measurements are given in Table 2.

The metal supplied in the form of a thin sheet can be characterized as a spheoridized annealed cold rolled 1020 steel. Figure 2 shows the microstructure containing grains of ferrite with spheoridized carbide particles located primarily at grain boundaries.

The bar stock steel is difficult to classify. Figure 3 shows microstructures at a depth of 0.18 inch below the surface and at the core. The ferrite and pearlite content up to a depth of 0.25 inches would classify the metal as a 1018 steel. However, the increased pearlite near the core makes the material more equivalent to a 1030 steel. This can be seen in the micrographs and in the hardness measurements listed in Table 2. Because of the variation in composition, this metal will be simply referred to as the bar steel.

---

*The metallurgical analysis was supplied by Mr. D. J. Borich of the Noise and Vibration Laboratory, General Motors Proving Ground.

EXPERIMENTAL EQUIPMENT AND SPECIMEN DESIGN

The closed-loop mechanical test system and testing techniques are similar to those described in Refs. 11 and 16. Figure 4 shows an over-all view of the equipment.

Specimen configurations for the sheet and bar steel samples are shown in Fig. 5. Figure 6 is a photograph of the bar steel specimen mounted in the load frame and the extensometer used to measure strain over a one-half inch gage length. This same extensometer also measured strains for the axial sheet steel specimens, Fig. 5b.

For the sheet steel it is necessary to choose a specimen configuration and loading fixture that will minimize the possibility of buckling. Both axial and transverse specimens, Figs. 5b and 5c, are mounted in two stages. First, each end of the specimen is mounted to one of the mounting fixtures (indicated by the letter "A") shown in Fig. 7. The rectangular slot of A is partially filled with Wood's metal, which is an alloy used with other types of specimen grips (11, 16). A fixture is heated until the Wood's metal melts. One end of the specimen is then placed in the slot. With one end of the specimen in the molten Wood's metal, an alignment device (B) is placed on the flat surface of the mounting fixture with its slot aligned with that of the fixture. In this position a portion of the specimen will be in the slot of B. The screw is slightly tightened and the fixture cooled. The other end of the specimen is mounted in the second fixture in the same manner. Second, this entire assembly is secured to the load frame and ram, Fig. 8.

The first fatigue tests of the sheet steel were performed on samples of the configuration shown in Fig. 5b. All specimens had rectangular gaged sections. For different specimens the width, W, varied from 0.070 to 0.4 inches and the

straight section length, L, from 0.25 to 0.5 inches. None of these configurations prevented buckling during 100 cycles of reversed strain limits of ±0.005. Marsh et al. (17) report fatigue test results for 1015 sheet steel specimens, machined from plates varying in thickness from 0.1 to 0.2 inches. Cyclic strain amplitudes up to ±0.0075 were obtained using specimens with straight cylindrical gaged sections.

Figure 5c shows the final specimen design. This design is similar to the hour glass shaped specimen which is commonly used for testing at large strain amplitudes. Slot et al. (18) tested hour glass shaped specimens under axial strain control. Total axial strain was computed from load and diametrical strain. The techniques discussed with regard to the transverse sheet steel specimens are similar to those in Ref. 18.

Figure 9 shows the transverse sheet steel fatigue specimen and the extensometer for measuring strains across the thickness of the specimen. The points of contact to the specimen from extensometer consist of a flat surface on one side and a point contact from a rounded surface on the other side. The thickness of the specimen is the gage length. For a 0.070 inch thick specimen, a strain of 0.02 would be a deformation of 0.0014 inch. To calibrate the extensometer for this small range of deformation, a micrometer was used that possessed a vernier scale for 0.0001 inch. Figure 10 shows the transverse extensometer on the calibrating fixture.

Equation 1 relates transverse strain, ϵ_{tr}, and total axial strain, ϵ.

$$\epsilon = \frac{\sigma}{E} - \frac{1}{\mu_p}\left[\epsilon_{tr} + \mu_e\left(\frac{\sigma}{E}\right)\right] \qquad (1)$$

where E is the elastic modulus, σ the stress, μ_e and μ_p the elastic and plastic Poisson's ratios, respectively. The quantity σ/E is the elastic component and

$1/\mu_p\,[\epsilon_t + \mu_e\,(\sigma/E)]$ the plastic component of total axial strain. A plastic Poisson's ratio of 1/2 was assumed, thus changing Eq. 1 to Eq. 2.

$$\epsilon = \frac{\sigma}{E} - 2\epsilon_{tr} - 2\mu_e\left(\frac{\sigma}{E}\right) \qquad (2)$$

For testing purposes, axial strain was obtained by programming an analog computer for Eq. 2. Figure 11 shows the analog circuit. Inputs to the circuit are the load, P, and the negative, $-\epsilon_{tr}$, of the transverse strain. The transverse strain gage was wired so that an expansion of the contact points produced a negative voltage output and contraction a positive output. Therefore, the transverse strain, ϵ_{tr}, is inverted upon entering the analog circuit.

By adjusting the value of the variable potentiometer, V_1, the analog equivalent of elastic strain, ϵ_e, can be obtained. To set V_1, a known dummy load is applied to the input of amplifier #1 before the specimen is mounted. By knowing the area of the specimen and elastic modulus, E, V_1 is adjusted for the desired analog output of amplifier #1. With the specimen mounted and cycling in the elastic range under load control, potentiometer V_2 is adjusted for zero output at amplifier #2. Amplifier #3 sums the elastic and plastic strains. From this circuit, total axial strain can be recorded and controlled directly.

The shape of the transverse sheet steel specimen, Fig. 5c, produces an uneven stress distribution across the mid-section. An elastic finite element program, ICES STRUDL, which is available on the 360/75 IBM Computer System at the University of Illinois, was used to determine this stress distribution. Figure 12 shows the finite element grid and Fig. 13 the computed stresses. A theoretical elastic stress concentration, K_t, of 1.3 was calculated.

STRESS-STRAIN BEHAVIOR

The monotonic and cyclic stress-strain data of both the sheet and bar steels are presented and discussed. Table 3 summarizes the entire testing program. Comparisons of the data for the two metals are made.

Monotonic Stress-Strain Behavior

One specimen of the bar steel and two specimens, one axial and one transverse, of the sheet steel were pulled in tension to fracture. The axial specimen, Fig. 5b, had a width of 0.127 inch and strain was measured over a gage length of 0.45 inch. The test results from these specimens determined the monotonic stress-strain properties. For each test, the displacement of the ram was controlled. Monotonic engineering stress-strain curves are shown in Figs. 14 and 15. Figure 14 shows the test results of both specimen configurations of the sheet steel. During initial loading the strain sensitivity is high enough to enable determination of the elastic modulus. At a strain of approximately 0.025, the strain sensitivity is reduced by a factor of ten for further recording of strain up to necking. Once necking occurs, the X-axis is switched to record the deflection of the ram and the Y-axis records the stress to fracture.

True* plastic strain, ϵ_p, versus true stress, σ, data are plotted in Figs. 16 and 17. Two least square approximations of the data for each plot are made. One line is to fit the relatively flat top portion of the stress-strain curve and the other line fits the more rapidly hardening segment. Each line is expressed in the form of Eq. 3.

$$\sigma = K(\epsilon_p)^n \tag{3}$$

*All engineering stress and strain data are converted to true stress and strain (11).

where:

K = Monotonic strength coefficient

n = Monotonic strain hardening exponent

Equation 3 can be rewritten as

$$\epsilon_p = (\frac{\sigma}{K})^{1/n} \qquad (3a)$$

Since the total strain, ϵ, is the sum of the components of elastic, σ/E, and plastic strain, the following equation can be written.

$$\epsilon = \frac{\sigma}{E} + (\frac{\sigma}{K})^{1/n} \qquad (4)$$

where E is the elastic modulus. Table 4 lists all the tension properties of both steels.

Least squares approximations for the data of both the transverse and axial sheet steel specimens are included in Fig. 16. Both specimens produced almost identical initial stress-strain behavior. The latter segments of the stress-strain curves and the final fracture properties of the two specimens were different.

Cyclic Stress-Strain Behavior

All test results for determining the cyclic stress-strain behavior of both steels were obtained under strain control. Figure 18 defines stress and strain ranges for a hysteresis loop as might be recorded during a test.

During cyclic loading, most metals undergo a transient period of cyclic hardening or softening. Both the sheet and bar steels will either cyclically harden or soften depending on the strain range. Figure 19 shows these phenomena for the bar steel. In Fig. 19a the strain amplitude is small enough so as to produce cyclic softening. For a larger strain amplitude, this same metal cyclically hardens, Fig. 19b. Figures 20 and 21 show the variation of stress with reversals of strain. The data

for Fig. 20 are obtained from the sheet specimens. A much more complicated situation is shown in Fig. 21 for the bar steel. Since the bar specimens exhibit an upper yield point, a large stress range can be initially obtained for a small strain range, which does not result in stresses that exceed the upper yield point. An example of this is shown in Fig. 22. The specimen was controlled between constant strain limits of ± 0.0013, producing an initial stress range below the lower yield strength. However, cyclic softening still occurred.

Although the material stress-strain response as shown in Figs. 20 and 21 is complicated, a relatively stable condition is reached during the initial portion of the life of each specimen. Morrow (10) describes this stable behavior in terms of a cyclic stress-strain curve, which is defined as a curve passing through the tips of a set of stable hysteresis loops. If the plastic strain and stress amplitude data for the cyclic curves are fitted by a straight line on a log-log plot, the curve may be described by an expression similar to Eq. 3 and 3a.

$$\frac{\Delta\sigma}{2} = K'\left(\frac{\Delta\epsilon_p}{2}\right)^{n'} \tag{5}$$

$$\frac{\Delta\epsilon_p}{2} = \left(\frac{\Delta\sigma/2}{K'}\right)^{1/n'} \tag{5a}$$

The (') denotes cyclic, therefore, K' is the cyclic strength coefficient and n' the cyclic strain hardening exponent. For total strain,

$$\frac{\Delta\epsilon}{2} = \frac{\Delta\sigma/2}{E} + \left(\frac{\Delta\sigma/2}{K'}\right)^{1/n'} \tag{6}$$

Equation 6 represents the stable cyclic stress-strain curve in terms of stress and strain ranges.

Landgraf et al. (13) suggest several experimental techniques for determining the cyclic stress-strain curve. The techniques applied to the sheet and bar steels include using companion specimens, incremental step strain test results, and monotonic tension after cyclic straining.

The companion specimen test results are those shown in Figs. 20 and 21. Representative stable data for each strain amplitude were taken at approximately one-half the fatigue life. Figure 23a shows the strain-time sequence for the incremental step strain spectrum. Maximum strain amplitudes are ± 0.015. Strain is increased or decreased in 40 increments. Figure 23b illustrates the resulting stress-strain response of the sheet steel. To obtain a stable condition before pulling in monotonic tension, the specimens were subjected to $1\frac{1}{2}$ blocks of the incremental step strain spectrum. By pulling the sample in monotonic tension a single curve is generated for the material in a stable condition.

Data for determining the cyclic stress-strain curves are plotted in Figs. 24 through 29. A straight line fit on the log-log coordinates for each set of data are made by the least squares method. The least squares lines for the companion specimen data are included in Figs. 26 through 29 for comparison.

Each method produced significantly different results. For both steels, the companion specimen line crossed that of the incremental step strain, Figs. 26 and 27. A smaller K' and n' resulted from the incremental step strain data. Figures 28 and 29 show a similar but even more pronounced situation for the precycled monotonic tension data. Comparisons of the cyclic stress-strain curves, as obtained by the three methods, are represented in Fig. 30. This large discrepancy between the data for the different methods does not exist for the higher strength metals cited in Ref. 13.

Figure 31 shows the stress response of the bar steel to a block strain spectrum. The first level consisted of 30 cycles of ±0.0125 strain, at the end of which the stress-strain behavior appeared stable. For each new strain amplitude, a transient period existed during which cyclic hardening or softening occurred. During the transient phase, the stress amplitudes varied as much as 8 ksi. This type of phenomenon continually occurs during incremental step straining. The monotonic tension after precycling is not characteristic of any one particular stable strain range. A stable condition is never actually reached, partially explaining the different results of the cyclic stress-strain curves.

However, for each technique, a close similarity exists between the two steels. Figure 32 shows this agreement. The cyclic properties of both steels are listed in Table 5.

The summary of the stress-strain data shown in Fig. 32, indicates that the bar steel properties would be an accurate approximation of those of the sheet steel. The choice of the appropriate method of determining the cyclic stress-strain curve will depend on the type of load history to be modeled.

FATIGUE RESISTANCE

Data pertinent to the ability of the sheet and bar steels to resist a fatigue environment are presented. Three types of test results generated these data:

(1) constant amplitude completely reversed strain,

(2) an initial cyclic overstrain followed by completely reversed strain, and

(3) initial and periodic cyclic overstrains between every 10^5 cycles of completely reversed strain.

The constant amplitude data are that shown in Figs. 20 and 21. Further data were generated with an initial overstrain and periodic overstrains. An example of the overstrain spectrum is represented in Fig. 33. This overstraining is similar to the decreasing portion of the incremental step strain spectrum. In this case, the sequence consisted of only twenty steps and a maximum strain of ± 0.01. One sheet and one bar specimen were strained according to the incremental step spectrum, similar to that shown in Fig. 23a, except the maximum strain and number of increments were the same as for the overstrain sequence. Both samples produced fatigue lives greater than sixty blocks. This would be equivalent to 120 overstrains, if the increasing and decreasing portions of each block are equally damaging.

Results of these tests in terms of strain and reversals to failure are presented in Figs. 34 through 39. Tables 6 through 11 list the fatigue test results and Table 12 gives the fatigue properties. Data for determining the strain components were taken from a stress-strain loop at approximately half the fatigue life. For the periodically overstrained samples, the representative loop was selected as that just before an overstrain. Large strain test results with no overstraining are also included with the overstrained data.

Total strain is separated into elastic and plastic components for the strain reversals to failure, $2N_f$, data. Elastic strain is computed by dividing the stress amplitude by the elastic modulus. Plastic strain is this elastic strain subtracted from the total strain.

A straight line is fitted to the elastic and plastic strain data, Figs. 34 through 39, by the least squares method. The elastic strain line has an equation of the form

$$\frac{\Delta\epsilon_e}{2} = \left(\frac{\sigma_f'}{E}\right)(2N_f)^b \tag{7}$$

where σ_f' is the fatigue strength coefficient and b is the fatigue strength exponent. For plastic strain

$$\frac{\Delta\epsilon_p}{2} = \epsilon_f'(2N_f)^c \tag{8}$$

where ϵ_f' is the fatigue ductility coefficient and c the fatigue ductility exponent. When added, Eqs. 7 and 8 form a relation between total strain and reversals to failure.

$$\frac{\Delta\epsilon}{2} = \left(\frac{\sigma_f'}{E}\right)(2N_f)^b + \epsilon_f'(2N_f)^c \tag{9}$$

The constants b and c are the respective slopes of the elastic and plastic strain lines. Values of σ_f'/E represent the elastic strain and ϵ_f' the plastic strain at $2N_f = 1$.

Data for the sheet steel specimens that were not subjected to any overstrains, Fig. 34, do not allow an accurate straight line fit. The major inconsistencies occur in the long life region. At small strain amplitudes, the sheet steel specimens experienced a shift of mean stress in either tension or compression. Due to the extremely small deflection range, any small change of the temperature or position on the specimen

of the extensometer resulted in relatively large strain changes. For the bar steel, Fig. 35, no mean stress shifts occurred. Figure 40a compares the fatigue resistance of both steels.

Initially overstrained data, Figs. 36 and 37, were generated to approximate the condition of the metal at the critical location of a structural member, which had been overloaded during the manufacturing process or early in its life. Included in Figs. 36 and 37 are the strain-life lines for the specimens which were not overstrained. Initial overstraining did not appreciably affect the sheet steel. Since the sheet steel was overstrained during the rolling process, one more additional overstrain would not be expected to reduce the fatigue life. The initial overstrain sequence applied to the bar specimens did increase the slopes of the strain-life lines, Fig. 37, indicating less resistance to fatigue loading. It might be anticipated that the fatigue resistance of the initially overstrained bar specimens would be similar to that of the sheet specimens. Figure 40b compares the initially overstrained strain-life lines for both steels. The resemblance is close.

Watson and Topper (19, 20) reported the same effect of overstrain on four other structural steels. One steel (20), with a yield stress of 84 ksi, was not affected by an overstrain. Overstraining was also shown (15, 21, 22) to reduce the fatigue lives of a 4340 alloy steel and 2024-T4 aluminum.

Since many structural members experience frequent overloads during normal service, the parameters used in the fatigue analysis of such structures should also reflect this type of loading. Test results with periodic overstrains every 10^5 cycles were obtained. The overstrains were the same as shown in Fig. 33. Strain-life data for this series of tests are represented in Fig. 38 for the sheet steel and Fig. 39 for the bar steel. The least square lines from the non-overstrained data are also included in the figures. Little difference exists between initial and periodic

overstrain data for the bar steel. Fatigue lives of the sheet steel are significantly reduced due to repeated overstraining. Figure 40c compares the periodically overstrained data for both steels. Due to the similarity thus far between the two steels, this sudden deviation was unexpected.

Dowling (21) reported a reduction in fatigue life of a 4340 alloy steel due to periodic overstraining every 10^5 cycles. It was observed that the metal would harden slightly at small strain ranges. By periodically overstraining, a softer condition could be obtained and, therefore, more plastic strain would be present throughout a greater portion of the fatigue life. The opposite situation was observed for both the sheet and bar steels. After each overstrain, a very small degree of hardening was observed. Therefore, no explanation for the effect of periodic overstraining on the sheet steel can be given.

The effect on the fatigue resistance due to mean stress was not investigated. Watson and Topper (19) reported fatigue data with mean stress for a 1015 steel, concluding that two parameters fit the data reasonably well. One mean stress parameter, proposed by Morrow (14), involves the fatigue strength coefficient, σ_f', and mean stress, σ_o.

$$(\frac{\Delta\sigma}{2})_{cr} = \frac{\Delta\sigma/2}{1 - \sigma_o/\sigma_f'} \qquad (10)$$

where $(\Delta\sigma/2)_{cr}$ is the equivalent value of stress amplitude which would be used to calculate the elastic strain from a strain-life diagram. Smith et al. (23) proposed a mean stress parameter which did not rely on any experimental fatigue constants.

$$(\frac{\Delta\sigma}{2})_{cr} \quad [\frac{\sigma_{max}\ \Delta\epsilon E}{2}]^{\frac{1}{2}} \qquad (11)$$

where σ_{max} is the maximum stress peak. Both relations were shown to be equally accurate correction factors for a SAE 1015 steel. Equations 10 and 11 would almost certainly prove reasonable corrections for the bar and sheet steels.

CONCLUDING REMARKS

The following comments can be made concerning the techniques for testing thin plate specimens, and the stress-strain behavior and the fatigue resistance of the sheet and bar steels.

(1) Successful testing of the sheet steel was acomplished with the specimen design shown in Fig. 5c.

(2) Transverse strains can be measured and converted to total axial strain with the aid of an analog computer.

(3) Companion specimen, incremental strain step, and precycled monotonic tension test results all produced significantly different properties for the cyclic stress-strain curve of both steels, Fig. 30.

(4) The stress-strain properties as determined by any one procedure are in close agreement for the two steels, Fig. 32.

(5) An initial overstrain and periodic overstrains resulted in similar reductions in fatigue life for the bar steel.

(6) Only periodic overstraining reduced the fatigue life of the sheet steel.

(7) The initial and periodic overstrain data of the bar steel are similar to the non-overstrained and initially overstrained data of the sheet steel, Fig. 40.

ACKNOWLEDGMENT

The author is indebted to Professor JoDean Morrow for providing the technical background and guidance which made this investigation possible. The author wishes to thank Messrs. J. R. Wiley, R. Isaacson, T. M. Johnson, and D. J. Borich, of the General Motors Proving Grounds, for their continuous support and helpful suggestions. Mr. R. A. Testin performed the finite element analysis of the sheet specimen, and Mr. D. F. Dittmer developed computer programs for data reduction and carried out the testing program on the bar steel.

Mrs. R. A. Mathine typed the manuscript, and Mr. H. T. James drafted the figures.

REFERENCES

1. S. S. Manson and M. H. Hirschberg, "Crack Initiation and Propagation in Notched Fatigue Specimens," Proceedings of the First International Conference on Fracture, The Japanese Society for Strength and Fracture of Materials, Vol. 1, Sendai, Japan, September 1965, pp. 479-498.

2. T. J. Dolan, "Nonlinear Response under Cyclic Loading Conditions," Proceedings of the Ninth Midwestern Mechanics Conference, Madison, Wisc., August 1965, pp. 3-21.

3. J. H. Crews, Jr., and H. F. Hardrath, "A Study of Cyclic Plastic Stresses at a Notch Root," Experimental Mechanics, Vol. 6, No. 6, June 1966, pp. 313-320.

4. JoDean Morrow, Fatigue Design Handbook, Society of Automotive Engineers, Vol. 4, 1968.

5. J. H. Crews, "Crack Initiation at Stress Concentrations as Influenced by Prior Local Plasticity," Achievement of High Fatigue Resistance in Metals and Alloys, ASTM STP 467, American Society for Testing and Materials, 1970, pp. 37-52.

6. JoDean Morrow, R. M. Wetzel, and T. H. Topper, "Laboratory Simulation of Structural Fatigue Behavior," Effect of Environment and Complex Load History on Fatigue Life, ASTM STP 462, American Society for Testing and Materials, 1970, pp. 74-91. See also: R. M. Wetzel, JoDean Morrow, and T. H. Topper, "Fatigue of Notched Parts with Emphasis on Local Stresses and Strains," Naval Air Development Center Report No. NADC-ST-6818, September 1968.

7. L. F. Impellizzeri, "Cumulative Damage Analysis in Structural Fatigue," Effects of Environment and Complex Load History on Fatigue Life, ASTM STP 462, American Society for Testing and Materials, 1970, pp. 40-68.

8. J. Schijve, "The Accumulation of Fatigue Damage in Aircraft Materials and Structures," AGARD-AG-157, Advisory Group for Aerospace Research & Development, North Atlantic Treaty Organization, January 1972.

9. J. F. Martin, T. H. Topper, and G. M. Sinclair, "Computer Based Simulation of Cyclic Stress-Strain Behavior with Applications to Fatigue," Materials Research and Standards, Vol. 11, No. 2, February 1971, p. 23. See also: J. F. Martin, T. H. Topper, and G. M. Sinclair, "Computer Based Simulation of Cyclic Stress Strain Behavior," T. &A. M. Report No. 326, Department of Theoretical and Applied Mechanics, University of Illinois, Urbana, July 1969. See also Chapter V of: T. H. Topper and JoDean Morrow, Editors, "Simulation of the Fatigue Behavior in Spectrum Loaded Notched Members," T. &A. M. Report No. 333, Department of Theoretical and Applied Mechanics, University of Illinois, Urbana, January 1970, (Final Report for Aero Structures Department, Naval Air Development Center).

10. JoDean Morrow, "Cyclic Plastic Strain Energy and Fatigue of Metals," Internal Friction, Damping, and Cyclic Plasticity, ASTM STP 378, American Society for Testing and Materials, 1965, pp. 45-87.

11. D. T. Raske and JoDean Morrow, "Mechanics of Materials in Low Cycle Fatigue Testing," Manual on Low Cycle Fatigue Testing, ASTM STP 465, American Society for Testing and Materials, 1969, pp. 1-25. See also: D. T. Raske and JoDean Morrow, "Appendix A - Low Cycle Fatigue Testing from the Mechanics of Materials Viewpoint," Appendix to Naval Air Development Center Report No. NADC-ST-6818, September 1968, pp. 39-71.

12. T. Endo and JoDean Morrow, "Cyclic Stress-Strain and Fatigue Behavior of Representative Aircraft Metals," Journal of Materials, Vol. 4, No. 1, March 1969, pp. 159-175. See also: T. Endo and JoDean Morrow, "Monotonic and Completely Reversed Cyclic Stress-Strain and Fatigue Behavior of Representative Aircraft Metals," Aeronautical Structures Laboratory Report No. NAEC-ASL-1105, June 1966.

13. R. W. Landgraf, JoDean Morrow, and T. Endo, "Determination of the Cyclic Stress-Strain Curve," Journal of Materials, Vol. 4, No. 1, March 1969, pp. 176-188.

14. J. C. Grosskreutz, "The Mechanisms of Metal Fatigue (I)," (Review Article), physica status solidi (b), Vol. 47, No. 1, 1971, pp. 11-31.

15. N. E. Dowling, "Fatigue Failure Predictions for Complicated Stress-Strain Histories," Journal of Materials, Vol. 7, No. 1, March 1972, pp. 71-87. See also: N. E. Dowling, "Fatigue Failure Predictions for Complicated Stress-Strain Histories," T. &A.M. Report No. 337, Department of Theoretical and Applied Mechanics, University of Illinois, Urbana, January 1971.

16. C. E. Feltner and M. R. Mitchell, "Basic Research on the Cyclic Deformation and Fracture Behavior of Materials," Manual on Low Cycle Fatigue Testing, ASTM STP 465, American Society for Testing and Materials, 1969, pp. 27-66.

17. G. M. March, A. D. Robb, and T. H. Topper, "Techniques and Equipment for Axial Fatigue Testing of Sheet Steel," SAE Paper 730578, presented at Automobile Engineering meeting, Detroit, Michigan, May 1973.

18. T. Slot, R. H. Stentz, and J. T. Berling, "Controlled-Strain Testing Procedures," Manual on Low Cycle Fatigue Testing, ASTM STP 465, American Society for Testing and Materials, 1969, pp. 100-128

19. P. Watson and T. H. Topper, "Fatigue Damage Evaluation for Mild Steel Incorporating Mean Stress and Overload Effects," Experimental Mechanics, Vol. 12, No. 1, January 1972, pp. 11-17.

20. P. Watson and T. H. Topper, "The Effects of Overstrain on the Fatigue Behaviour of Five Steels," presented at Fall meeting of the Metallurgical Society, Cleveland, Ohio, October 1970.

21. N. E. Dowling, "Fatigue Life and Inelastic Strain Response under Complex Histories for an Alloy Steel," Journal of Testing Evaluation, Vol. 1, No. 4, July 1973, pp. 271-287. See also: N. E. Dowling, "Fatigue Life and Inelastic Strain Response under Complex Histories for an Alloy Steel," T. & A. M. Report No. 354, Department of Theoretical and Applied Mechanics, University of Illinois, Urbana, April 1972.

22. T. H. Topper and B. I. Sandor, "Effects of Mean Stress and Prestrain on Fatigue Damage Summation," Effects of Environment and Complex Load History on Fatigue Life, ASTM STP 462, American Society for Testing and Materials, 1970, pp. 93-104. See also: T. H. Topper and B. I. Sandor, "Effects of Mean Stress on Fatigue Damage Summation," T. &A. M. Report No. 318, Department of Theoretical and Applied Mechanics, University of Illinois, Urbana, August 1968. See also Chapter III of: T. H. Topper and JoDean Morrow, Editors, "Simulation of the Fatigue Behavior in Spectrum Loaded Notched Members," T. &A. M. Report No. 333, Department of Theoretical and Applied Mechanics, University of Illinois, Urbana, January 1970, (Final Report for Aero Structures Department, Naval Air Development Center).

23. K. N. Smith, P. Watson, and T. H. Topper, "A Stress-Strain Function for the Fatigue of Metals," Journal of Materials, Vol. 5, No. 4, December 1970, pp. 767-776.

24. G. E. Dieter, Jr., Mechanical Metallurgy, McGraw-Hill Book Company, Inc., New York, 1961, pp. 251-252.

TABLE 1

CHEMICAL COMPOSITION OF THE SHEET AND BAR STEELS

Element	Sheet Steel	Bar Steel
Carbon	0.20	0.17(1)
		0.28(2)
Manganese	0.41	0.50
Phosphorus	0.010	0.008
Sulfur	0.011	0.010
Silicon	0.058	0.010
Aluminum	0.043	0.006
Chromium	0.01	0.04
Nickel	0.04	0.03
Niobium	< 0.005	< 0.005

(1) Average amount of carbon to a depth of $\frac{1}{4}$ inch from the surface.

(2) Average amount of carbon at the core.

TABLE 2

HARDNESS MEASUREMENTS OF SHEET AND CYLINDRICAL BAR STEEL

	Sheet Steel	Bar Steel
Microhardness (DPH)	123 ± 2	120 ± 2[1]
		145 ± 2[2]
Equivalent Rockwell B	62 ± 1	60 ± 1[1]
		73 ± 1[2]

(1) Hardness measurement taken at a depth of 0.18 inch below surface of bar.

(2) Hardness measurement taken at the core.

TABLE 3

OUTLINE OF TESTING PROGRAM

Type	Test	Remarks
Monotonic Tension properties	(1) Monotonic tension under stroke control	Both configurations
Steady State cyclic stress-strain properties	(1) Constant strain	Constant strain controlled tests were also used for data for fatigue resistance
	(2) Incremental step	
	(3) Monotonic tension after incremental step	
Fatigue resistance	(1) Constant amplitude strain control	Overstraining was accomplished by decreasing incremental step test
	(2) Initial overstrain followed by constant amplitude strain control	
	(3) Constant strain control with overstraining every 10^5 cycles	

TABLE 4

MONOTONIC TENSION PROPERTIES

	Sheet Steel		
	Axial	Transverse	Bar Steel
Modulus of Elasticity, ksi	27,000	30,000	30,000
Upper Yield Strength, ksi	-	-	50
Lower Yield Strength, ksi	-	-	42
0.2% Offset Yield Strength, ksi	37	37	42
Ultimate Strength, ksi	57	62	66
True Fracture Strength, ksi(1)	113/96	100/89	128/111
Strength Coefficient, ksi(2)	58/97	56/117	49/120
Percent Reduction in Area, %	64	49	59
True Fracture Ductility	1.02	0.67	0.90
Strain Hardening Exponent(2)	0.072/0.198	0.067/0.273	0.024/0.228

(1) The first value is the final load at fracture divided by the final cross-sectional area at fracture. The second value is corrected for triaxial stress due to necking as proposed by Bridgman (24).

(2) The first value represents the initial portion of the stress-strain curve (approximately up to 0.02 strain). The second value represents the remainder to the curve.

TABLE 5

STABLE CYCLIC STRESS-STRAIN PROPERTIES

	Sheet Steel	Bar Steel
Cyclic Strength Coefficient, ksi[1]	202/109/70	209/134/88
Cyclic Strain Hardening Exponent[1]	0.288/0.167/0.105	0.283/0.204/0.135

(1) The values represent those obtained by companion specimen, incremental strain step, and precycled monotonic tension test results, respectively.

TABLE 6

COMPLETELY REVERSED STRAIN CONTROLLED
TEST RESULTS OF THE SHEET STEEL

Total Strain Amplitude $\Delta\epsilon/2$[(1)]	Total Stress Amplitude $\Delta\sigma/2$, ksi[(2)]	Plastic Strain $\Delta\epsilon_p/2$[(1)]	Reversals to Failure $2N_f$
0.00785	46.4	0.00630	3,480
0.00535	42.0	0.00387	6,690
0.00259	30.4	0.00158	49,400
0.00200	28.4	0.00105	126,000
0.00160	24.7	0.00077	194,000
0.00134	22.1	0.00061	484,000
0.00107	19.9	0.00040	3,840,000
0.00081	20.3	0.00014	4,480,000

(1) Fifth place after the decimal is an estimation.

(2) First place after the decimal is an estimation.

TABLE 7

COMPLETELY REVERSED STRAIN CONTROLLED
TEST RESULTS OF THE BAR STEEL

Total Strain Amplitude $\Delta\epsilon/2$ [1]	True Stress Amplitude $\Delta\sigma/2$, ksi [2]	Plastic Strain $\Delta\epsilon_p/2$ [1]	Reversals to Failure $2N_f$
0.01545	55.5	0.01360	496
0.01034	54.0	0.00854	1,900
0.00778	51.1	0.00607	2,600
0.00513	45.7	0.00361	5,590
0.00334	40.5	0.00198	34,300
0.00231	32.8	0.00121	139,000
0.00174	26.8	0.00084	326,000
0.00159	26.1	0.00072	580,000
0.00125	22.8	0.00049	1,500,000

(1) Fifth place after the decimal is an estimation.

(2) First place after the decimal is an estimation.

TABLE 8

INITIALLY OVERSTRAINED TEST RESULTS
OF THE SHEET STEEL

Total Strain Amplitude $\Delta\epsilon/2$ [1]	True Stress Amplitude $\Delta\sigma/2$, ksi [2]	Plastic Strain $\Delta\epsilon_p/2$ [1]	Reversals to Failure $2N_f$
0.00106	20.4	0.00038	634,000
0.00081	19.3	0.00018	6,330,000

TABLE 9

INITIALLY OVERSTRAINED TEST RESULTS
OF THE BAR STEEL

Total Strain Amplitude $\Delta\epsilon/2$ [1]	True Stress Amplitude $\Delta\sigma/2$, ksi [2]	Plastic Strain $\Delta\epsilon_p/2$ [1]	Reversals to Failure $2N_f$
0.00200	29.3	0.00102	147,000
0.00125	23.0	0.00048	500,000
0.00107	22.0	0.00030	did not fail

(1) Fifth place after the decimal is an estimation.

(2) First place after the decimal is an estimation.

TABLE 10

PERIODICALLY OVERSTRAINED TEST RESULTS
OF THE SHEET STEEL

Total Strain Amplitude $\Delta\epsilon/2$[1]	True Stress Amplitude $\Delta\sigma/2$, ksi[2]	Plastic Strain $\Delta\epsilon_p/2$[1]	Reversals to Failure $2N_f$
0.00108	19.5	0.00043	464,000
0.00081	20.5	0.00013	1,070,000
0.00081	21.2	0.00011	1,470,000

TABLE 11

PERIODICALLY OVERSTRAINED TEST RESULTS
OF THE BAR STEEL

Total Strain Amplitude $\Delta\epsilon/2$[1]	True Stress Amplitude $\Delta\sigma/2$, ksi[2]	Plastic Strain $\Delta\epsilon_p/2$[1]	Reversals to Failure $2N_f$
0.00136	23.0	0.00059	324,000
0.00121	23.8	0.00042	560,000
0.00105	21.1	0.00035	1,880,000

(1) Fifth place after the decimal is an estimation.

(2) First place after the decimal is an estimation.

TABLE 12

FATIGUE PROPERTIES

	Sheet Steel	Bar Steel
Fatigue Strength Coefficient, ksi[1]	119/130/153	128/134/140
Fatigue Ductility Coefficient[1]	0.207/0.270/1.31	0.160/0.240/0.242
Fatigue Strength Exponent[1]	-0.121/-0.130/-0.147	-0.118/-0.125/-0.131
Fatigue Ductility Exponent[1]	-0.447/-0.478/-0.637	-0.412/-0.462/-0.465

(1) The values represent those obtained from non-overstrained, initial cyclic overstrain, and periodic cyclic overstrain data, respectively.

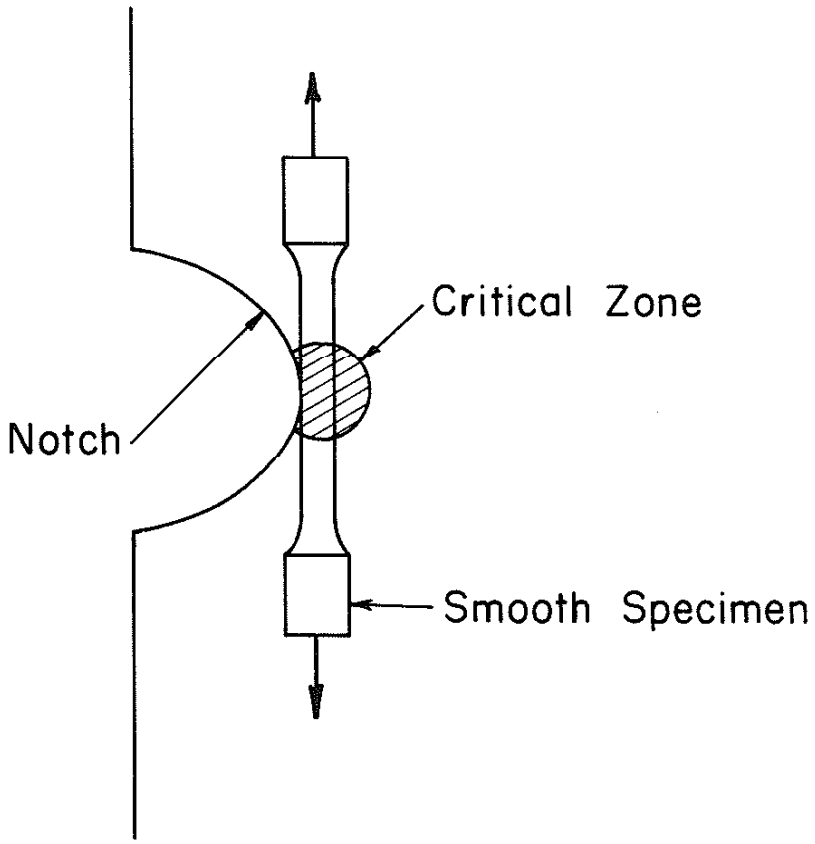

Fig. 1 Smooth Specimen Representation of Material at the Critical Zone

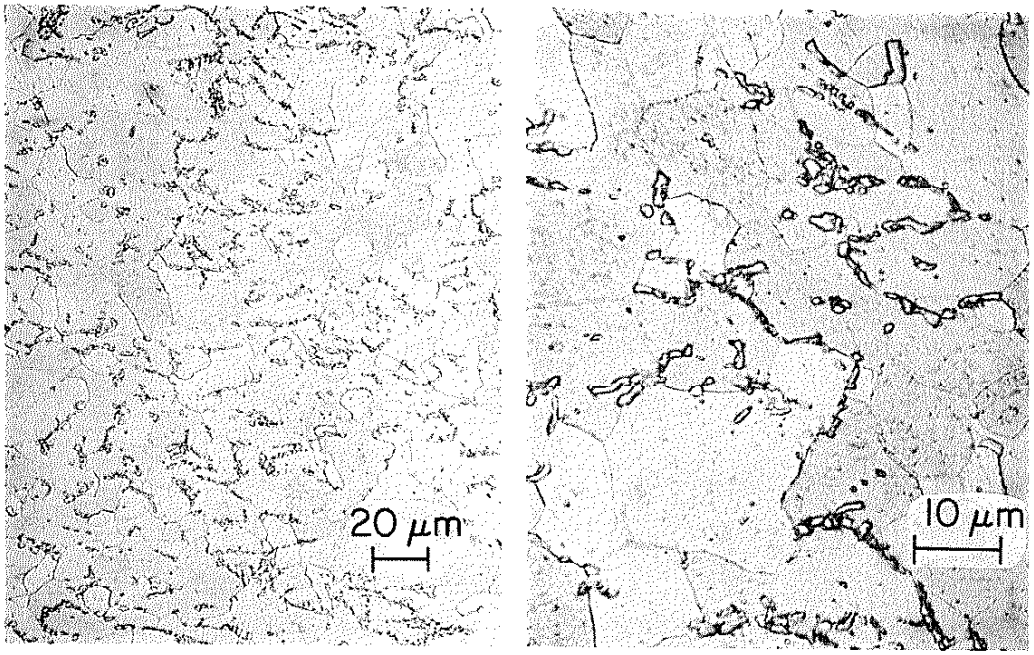

(a) (b)

Fig. 2 Microstructure of Spheoridized Annealed Cold Rolled 1020 Sheet Steel

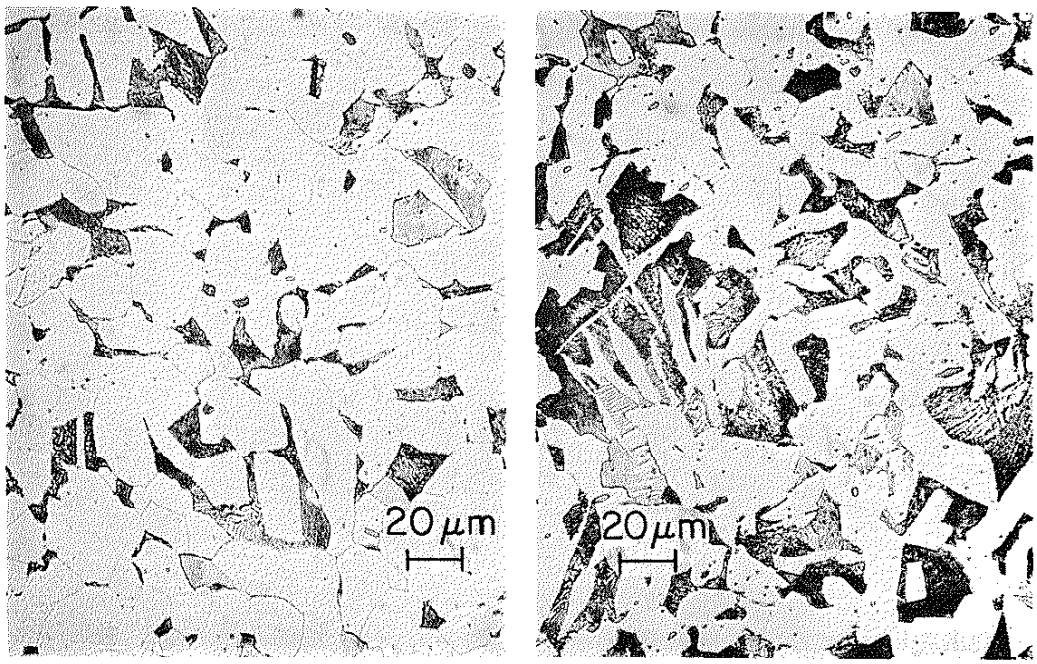

(a) 0.18 Inch from Surface (b) Core

Fig. 3 Microstructure of 3/4 Inch Diameter Bar Steel

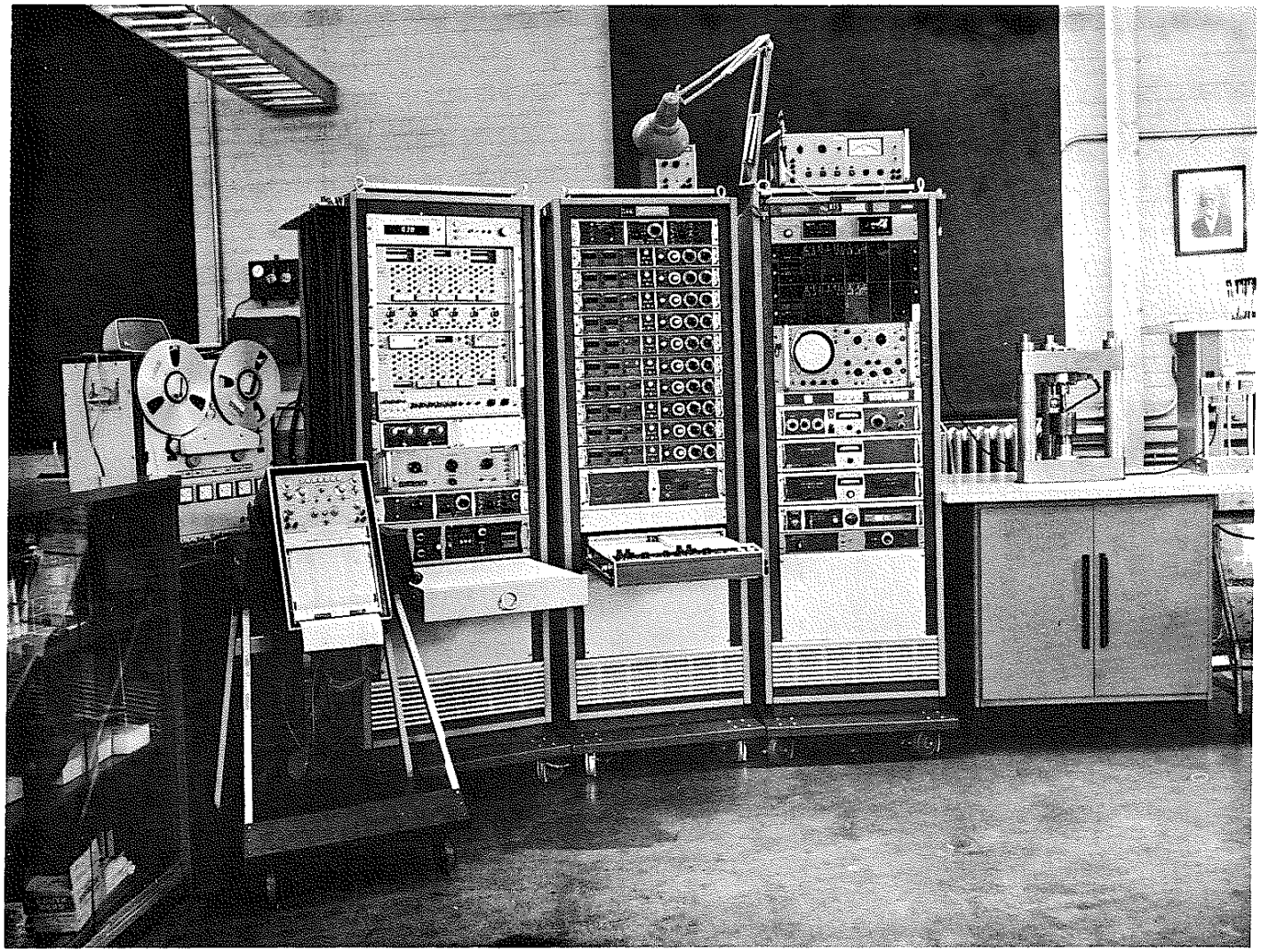

Fig. 4 Mechanical Test System

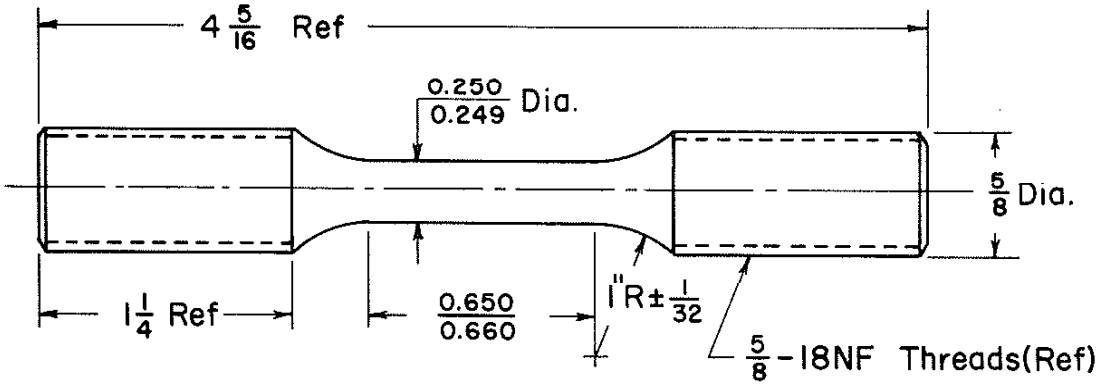

(a) Bar Steel Fatigue Specimen

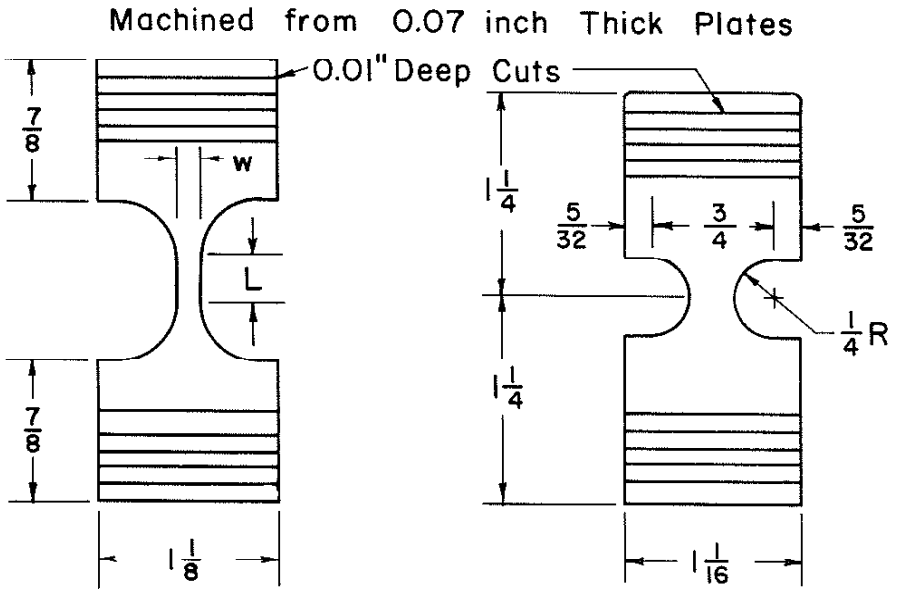

(b) Sheet Steel Axial Specimen

(c) Sheet Steel Transverse Specimen

Fig. 5 Specimen Configurations

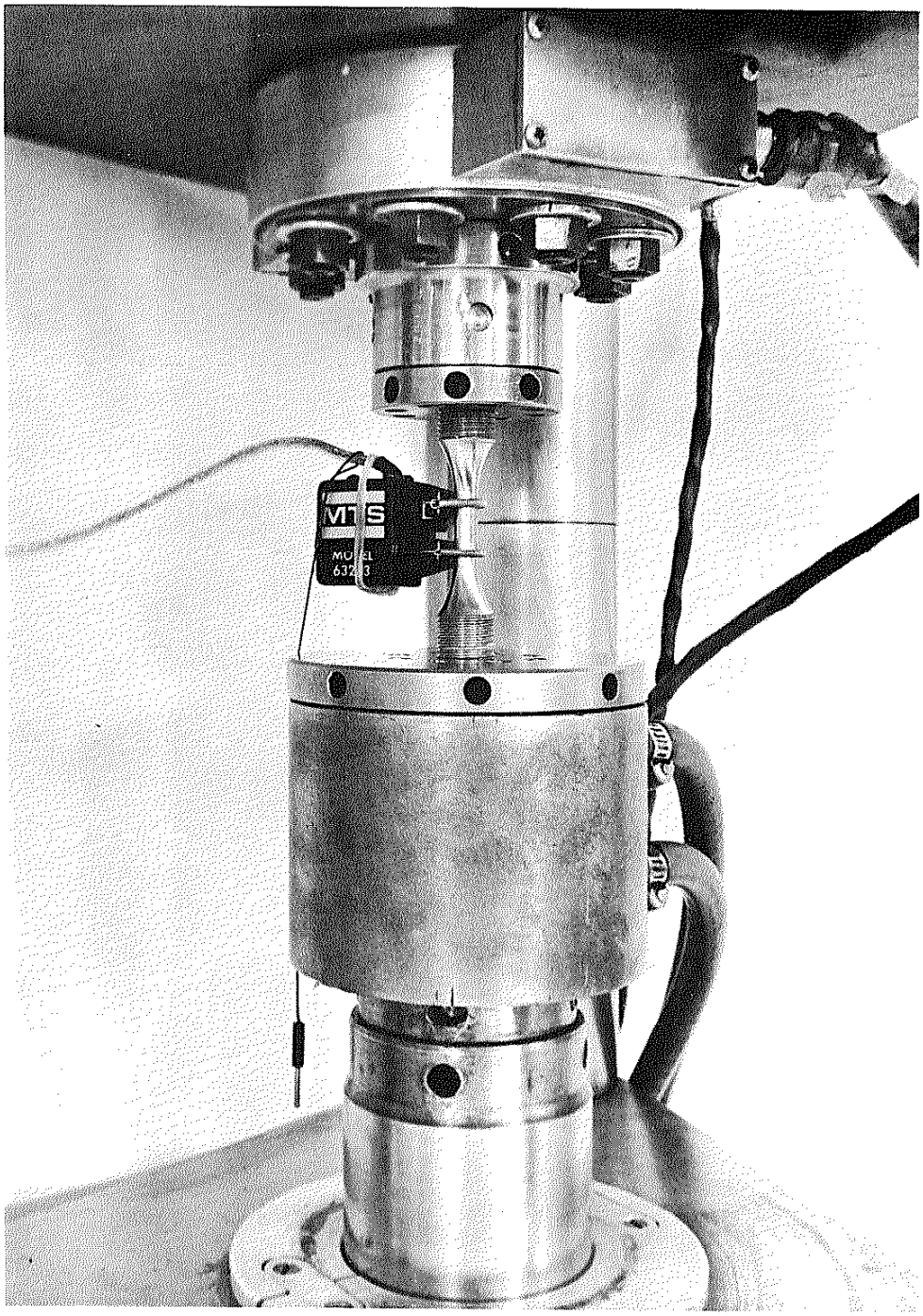

Fig. 6 Bar Steel Specimen Mounted in Load Frame and Extensometer

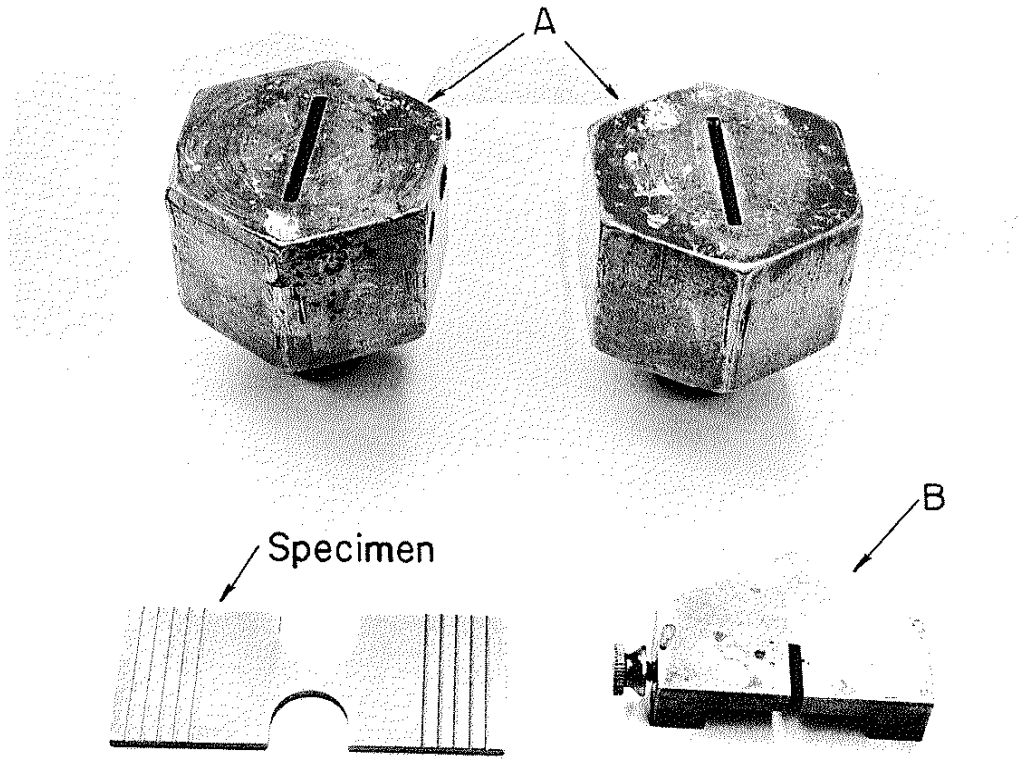

Fig. 7 Mounting Fixtures - Sheet Steel Specimens

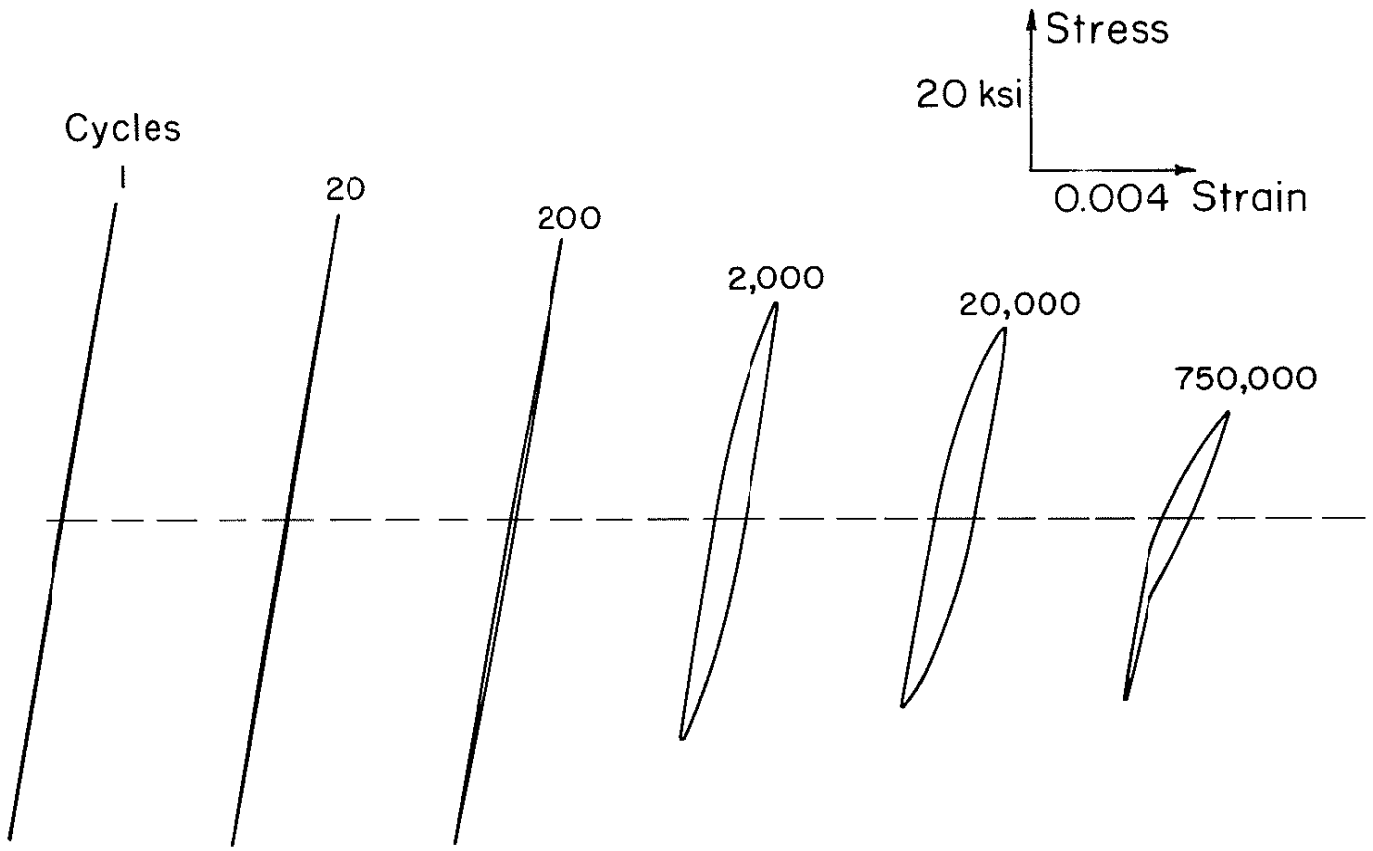

Fig. 22 Example of Cyclic Softening of the Bar Steel during a Constant Strain of $\Delta\epsilon/2 = \pm 0.0013$

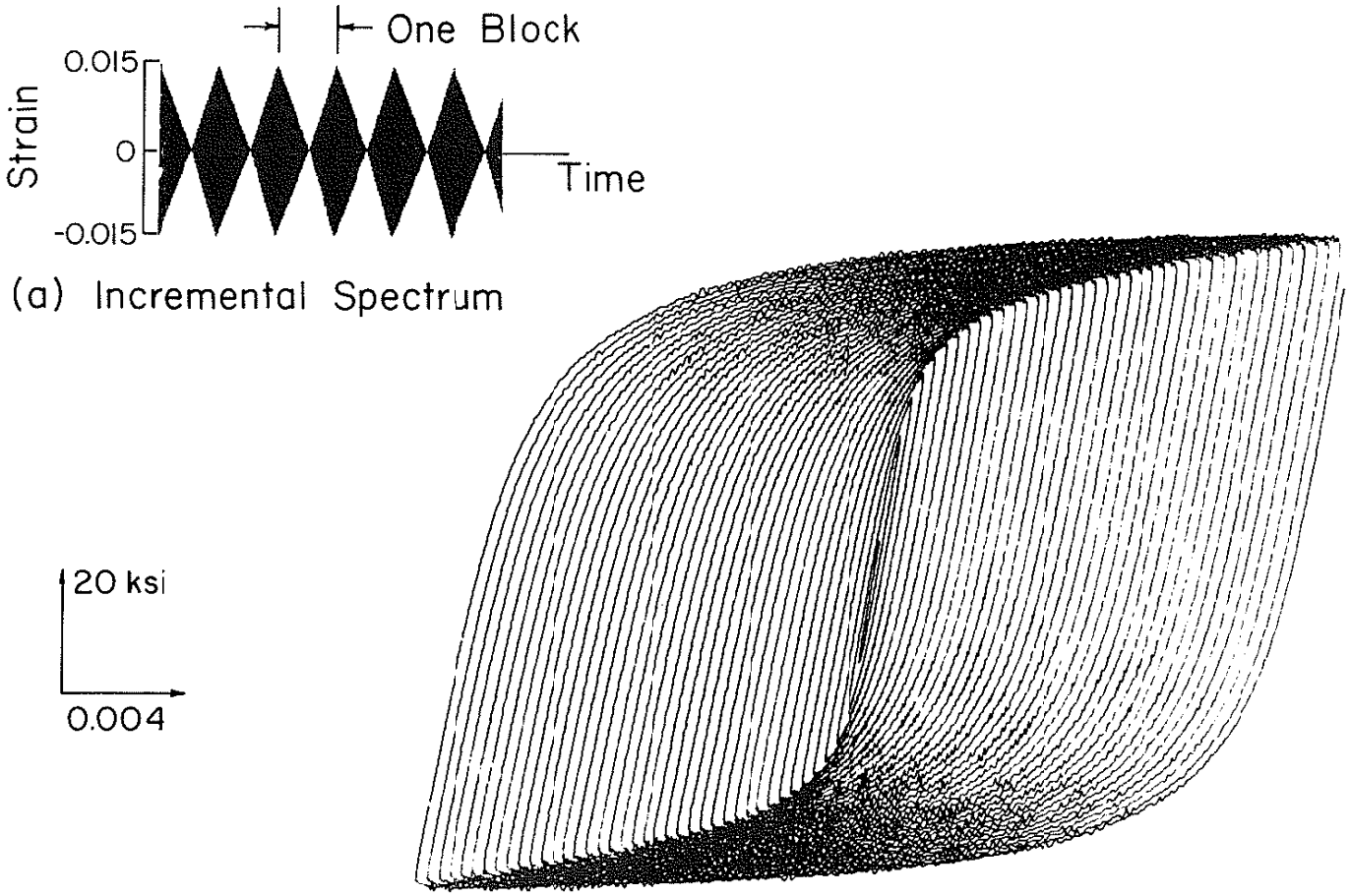

Fig. 23 Incremental Step Straining of Sheet Steel

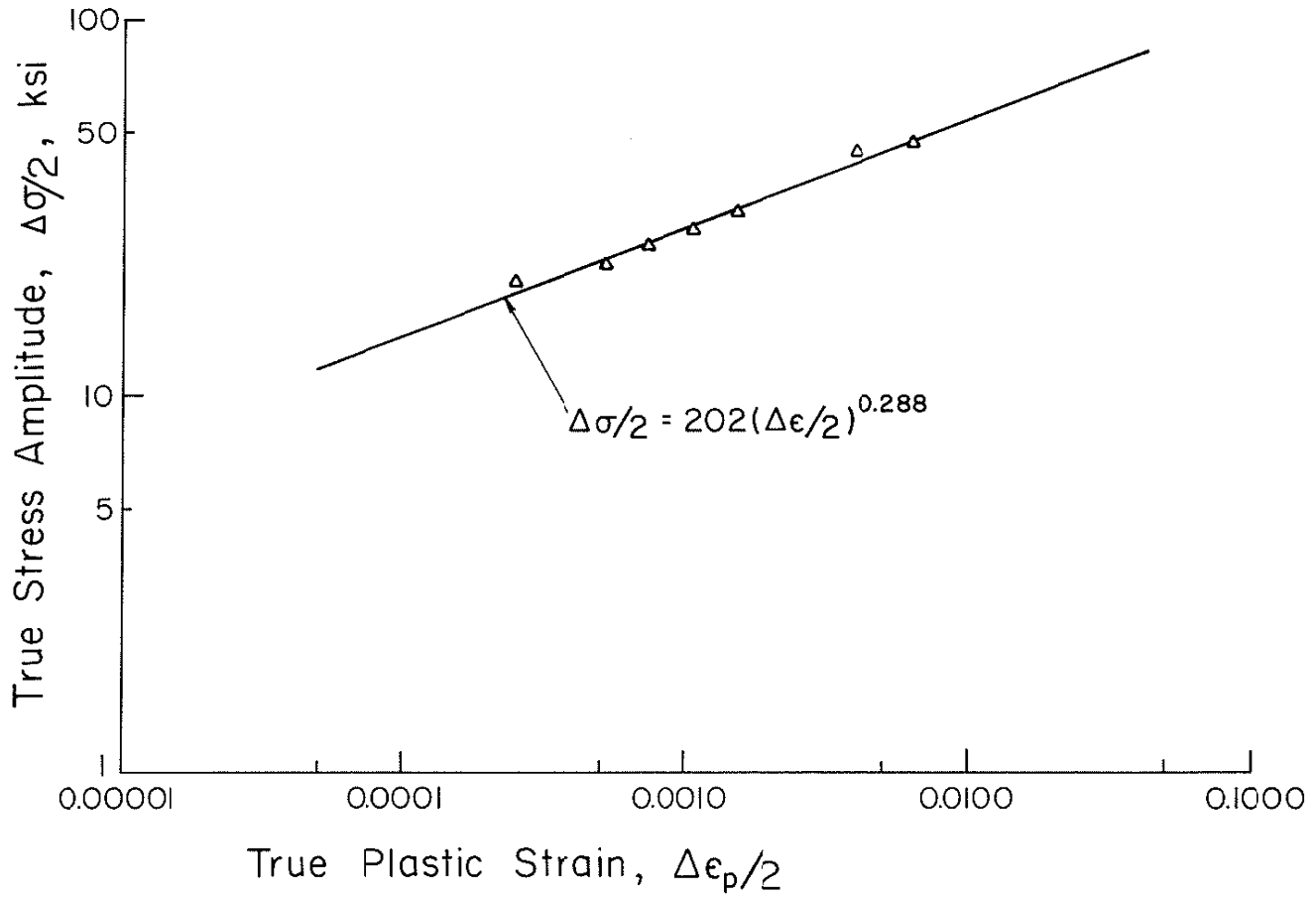

Fig. 24 Stress–Plastic Strain Data from Companion Specimens of the Sheet Steel

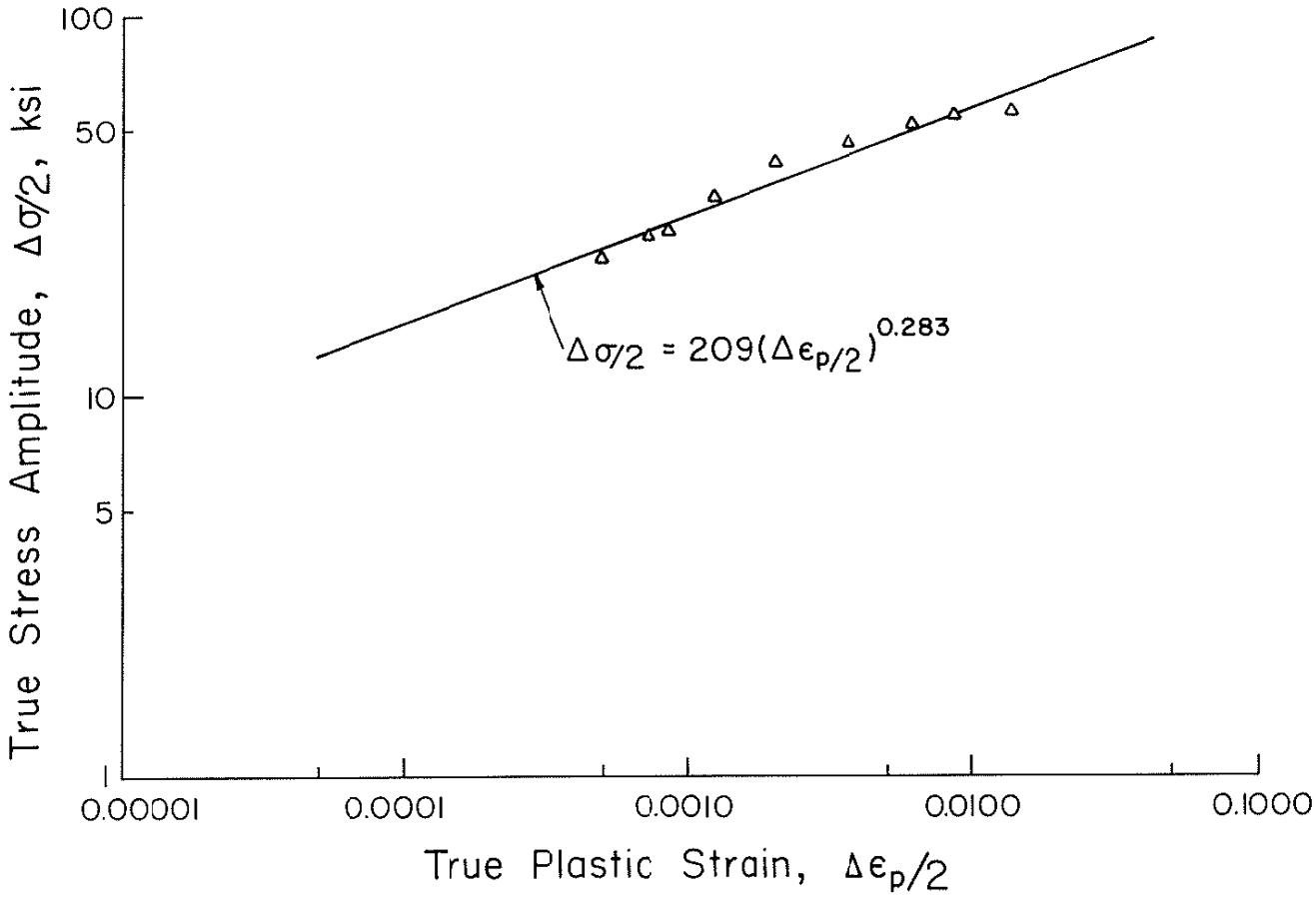

Fig. 25 Stress-Plastic Strain Data from Companion Specimens of the Bar Steel

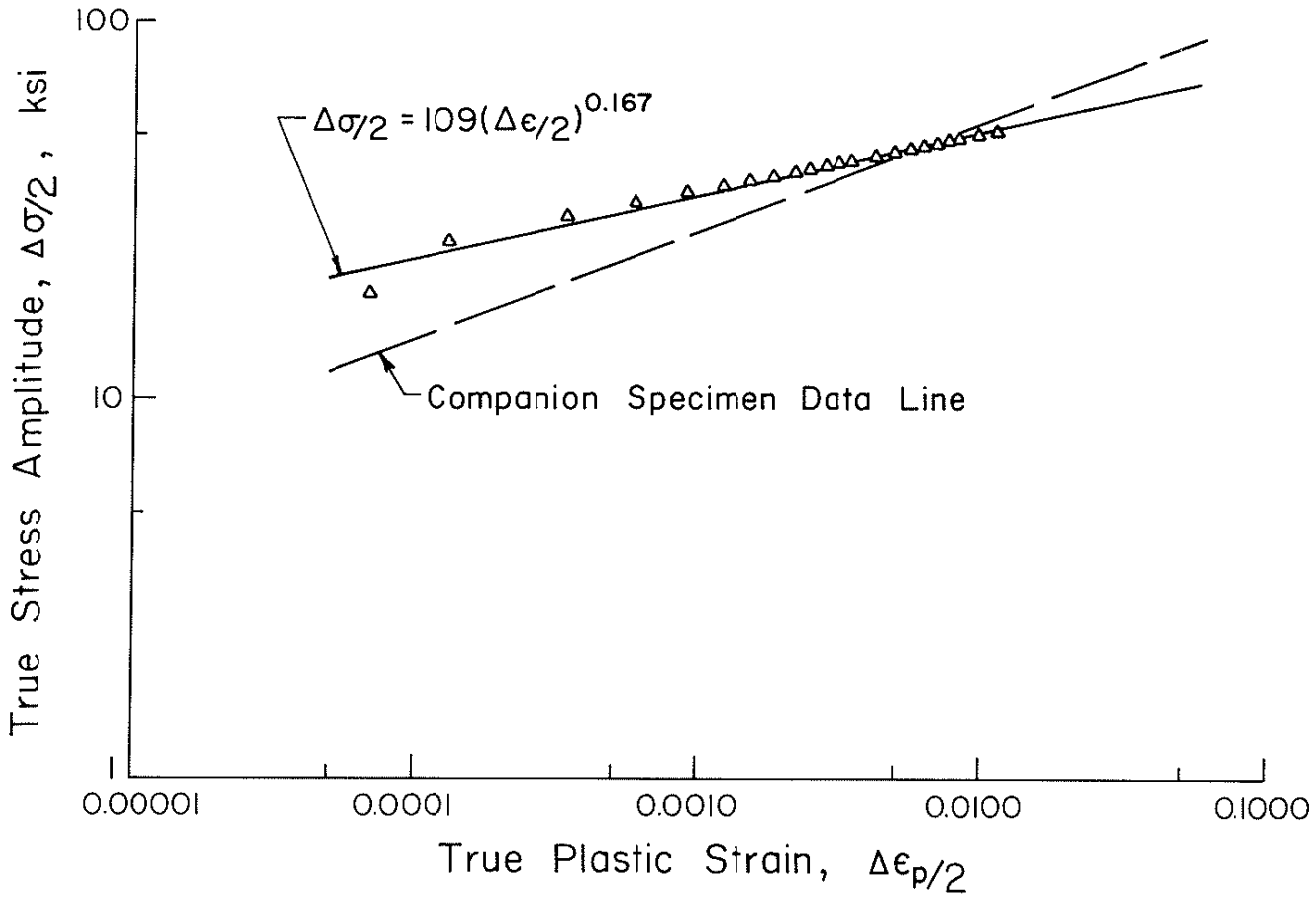

Fig. 26 Stress-Plastic Strain Data from Incremental Step Strain Test Results of the Sheet Steel

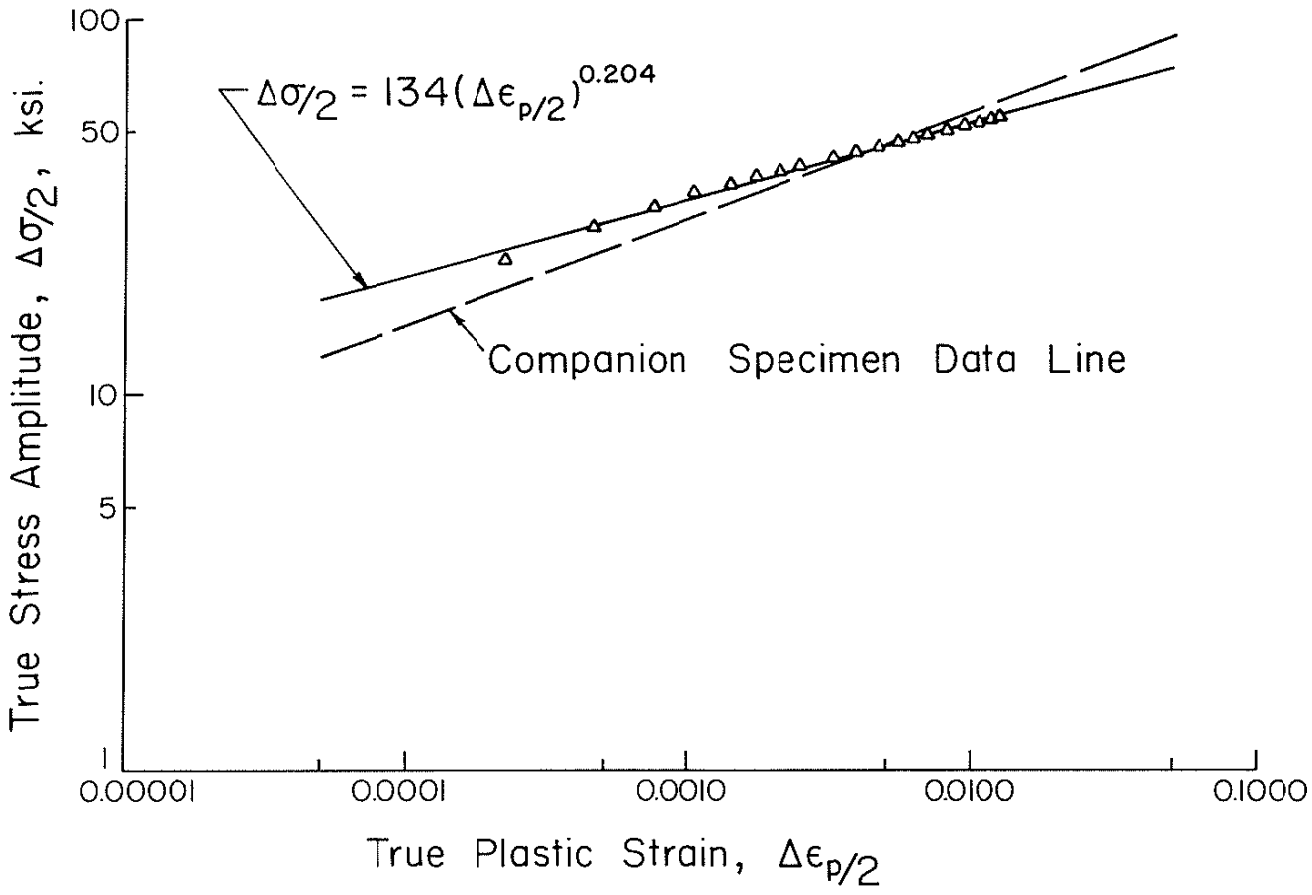

Fig. 27 Stress – Plastic Strain Data from Incremental Step Strain Test Results of the Bar Steel

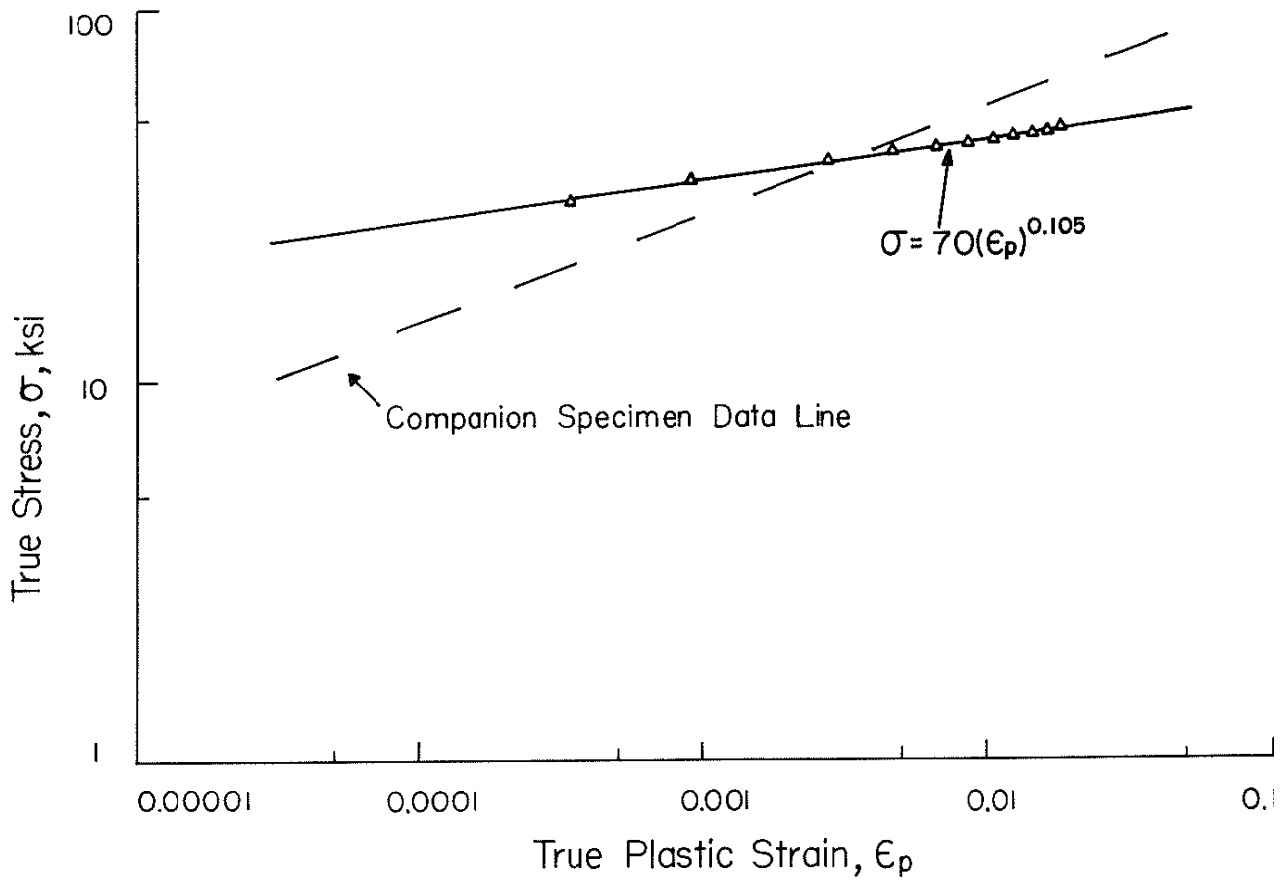

Fig. 28 Stress–Plastic Strain Data for Monotonic Tension after Incremental Step Straining of the Sheet Steel

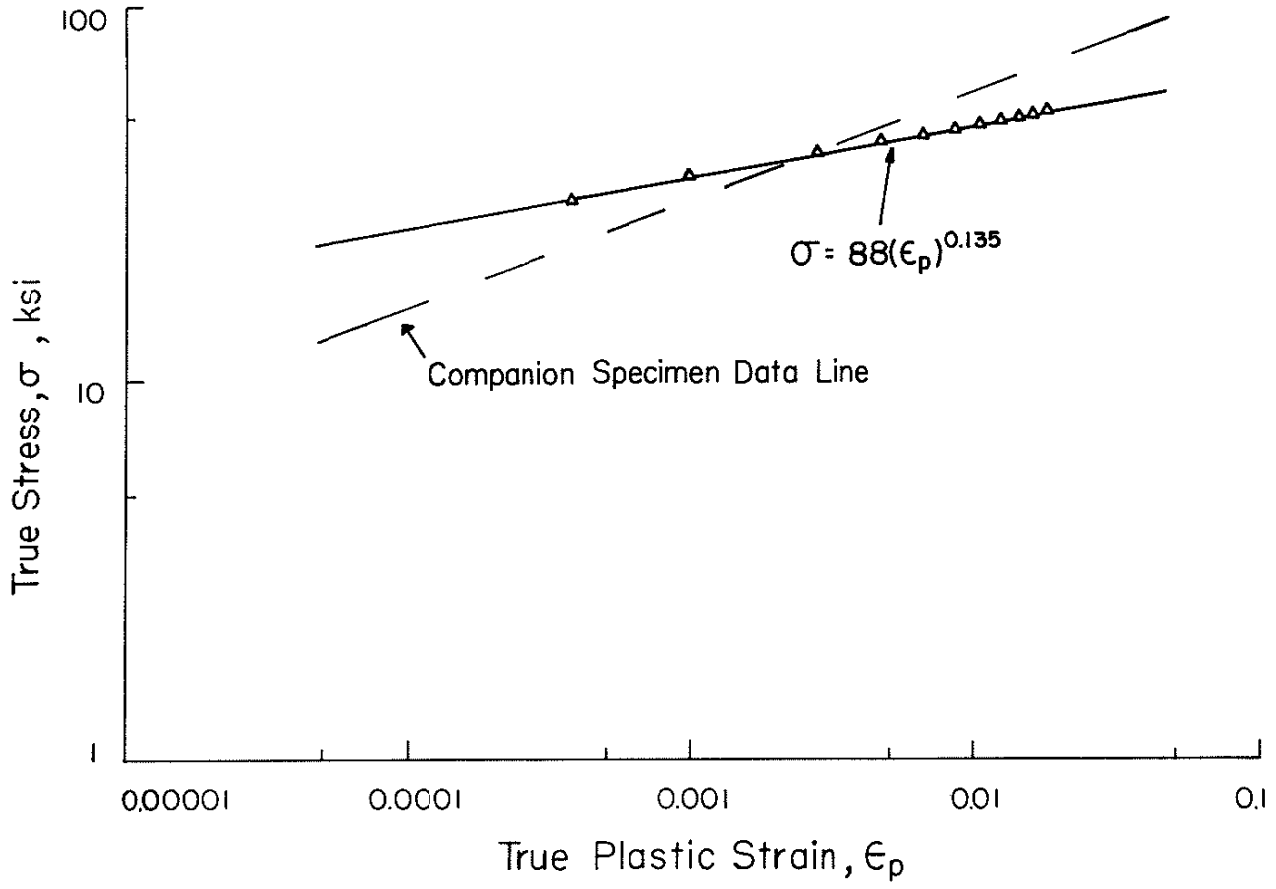

Fig. 29 Stress–Plastic Strain Data for Monotonic Tension after Incremental Step Straining of the Bar Steel

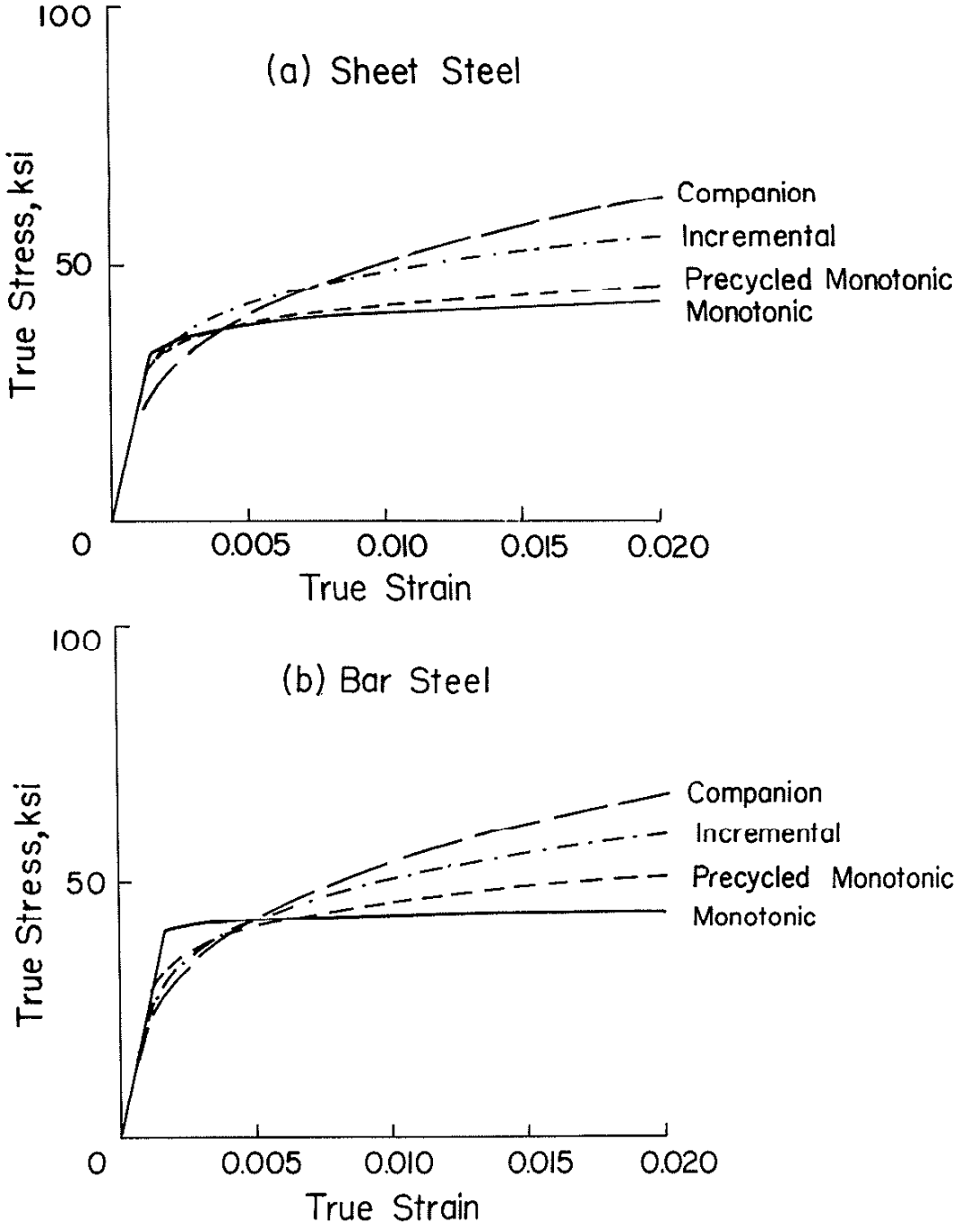

Fig. 30 Monotonic and Cyclic Stress-Strain Curves

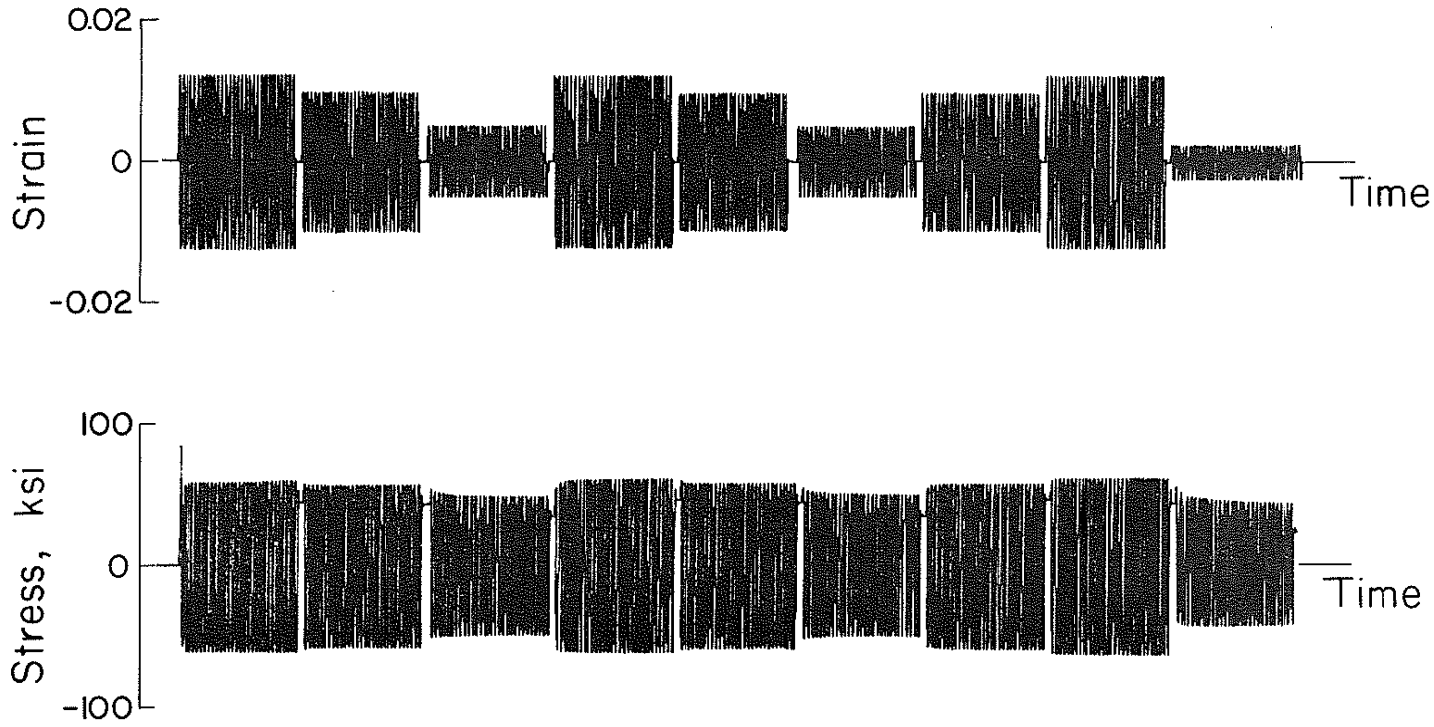

Fig. 31 Strain Control Block Test Results of Bar Steel

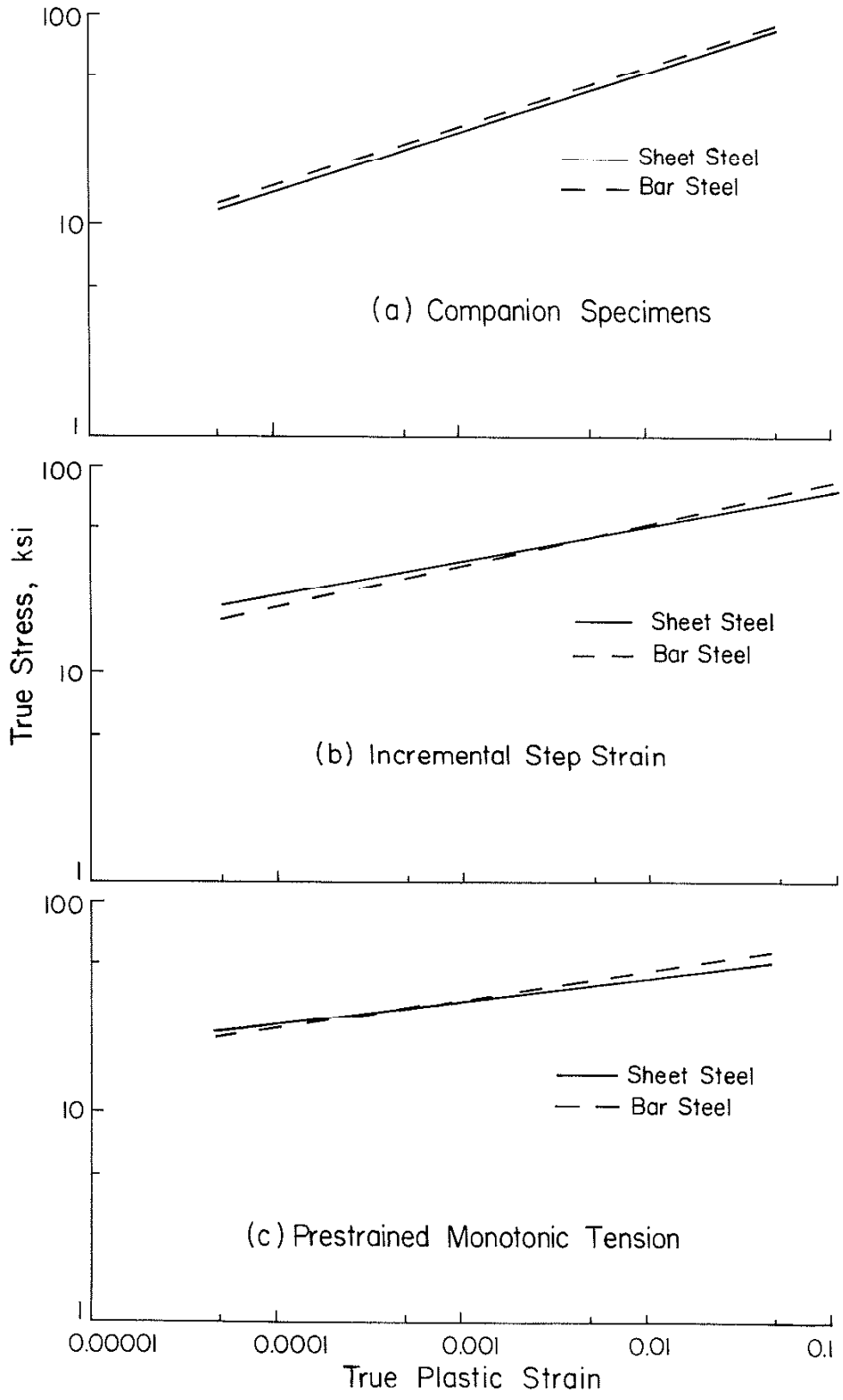

Fig. 32 Comparison of Least Squares Approximation of Cyclic Stress-Plastic Strain Curves for Both Steel

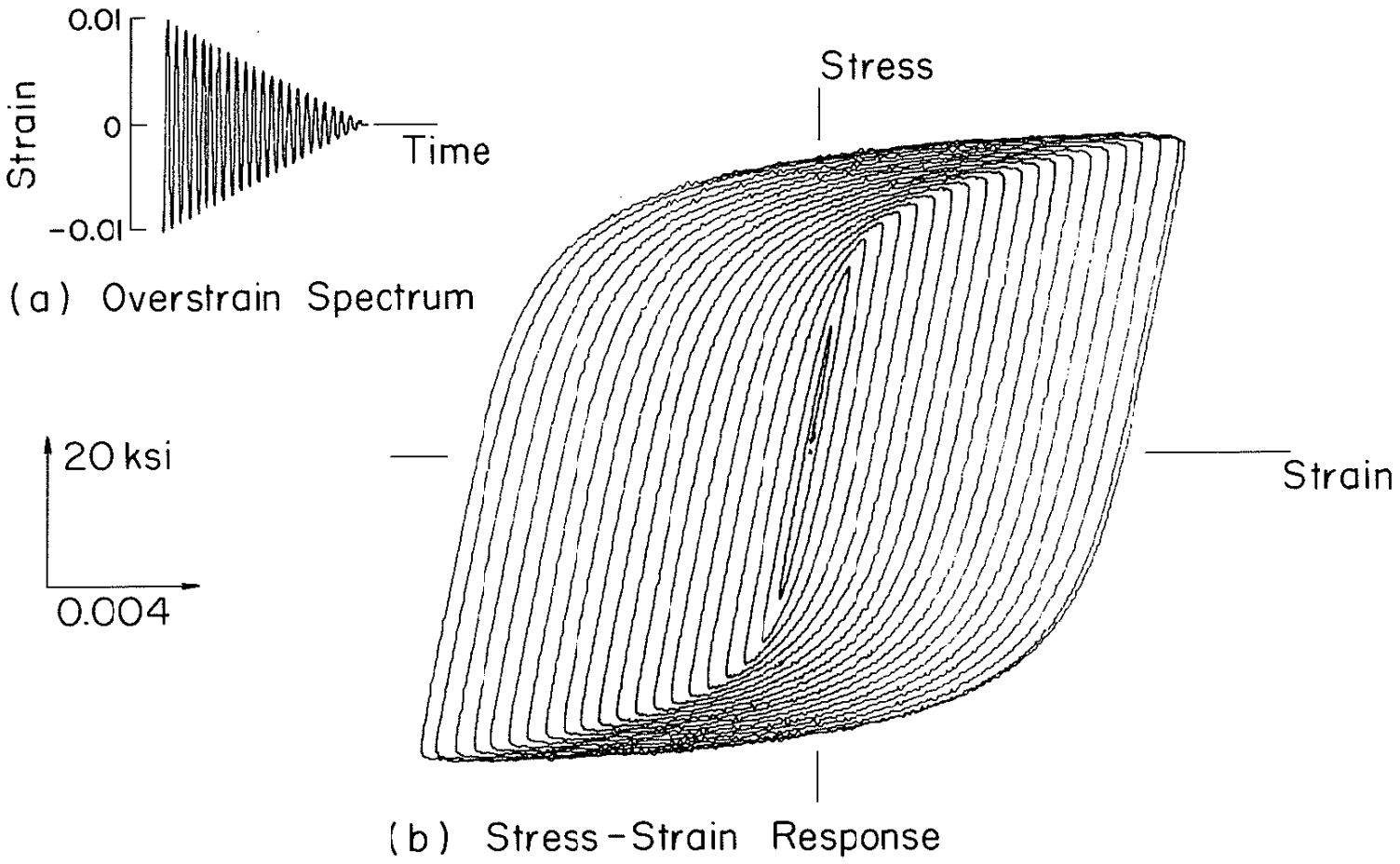

Fig. 33 Overstrain of Sheet Steel

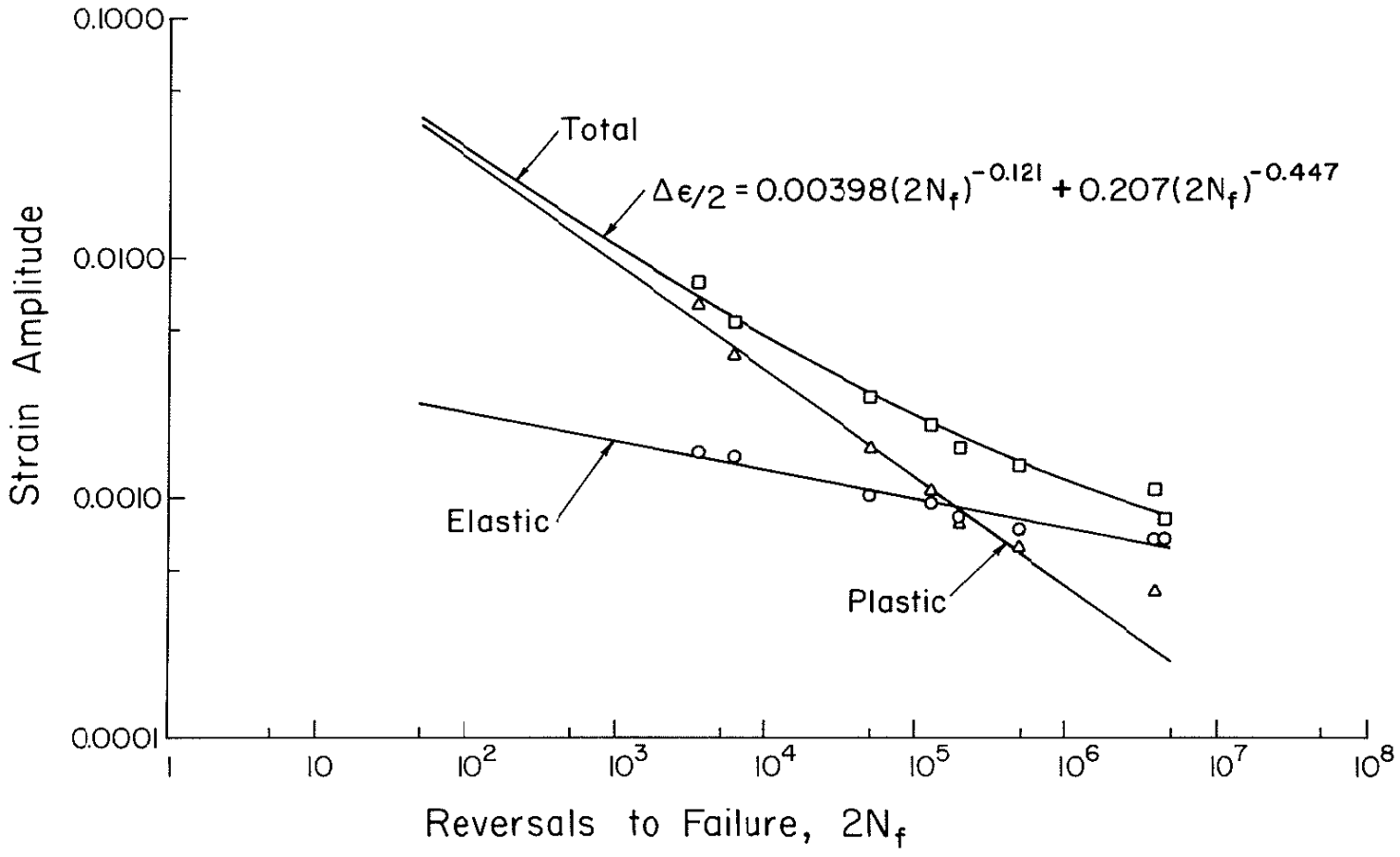

Fig. 34 Strain-Reversals to Failure Data for Sheet Steel

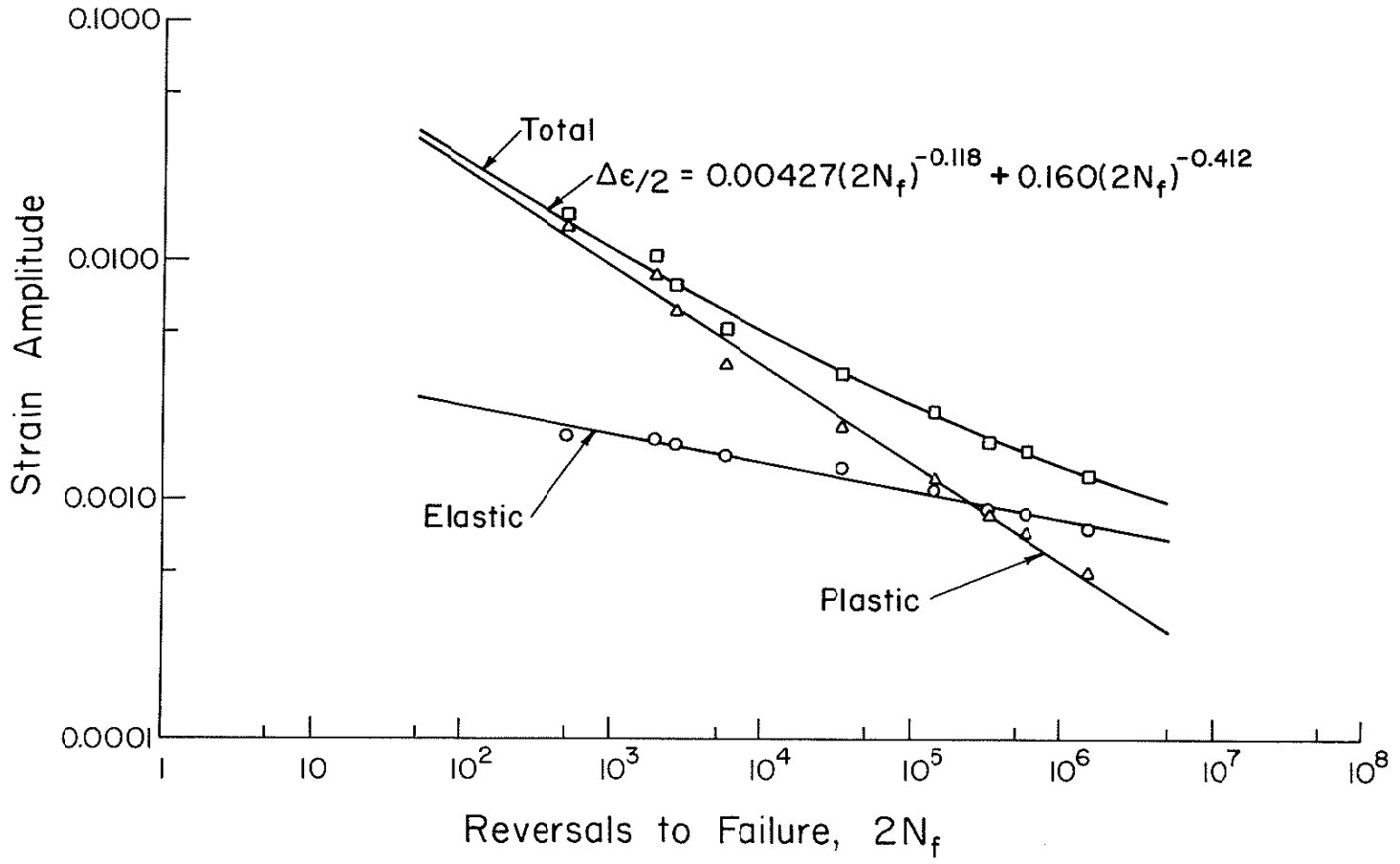

Fig. 35 Strain–Reversals to Failure Data for Bar Steel

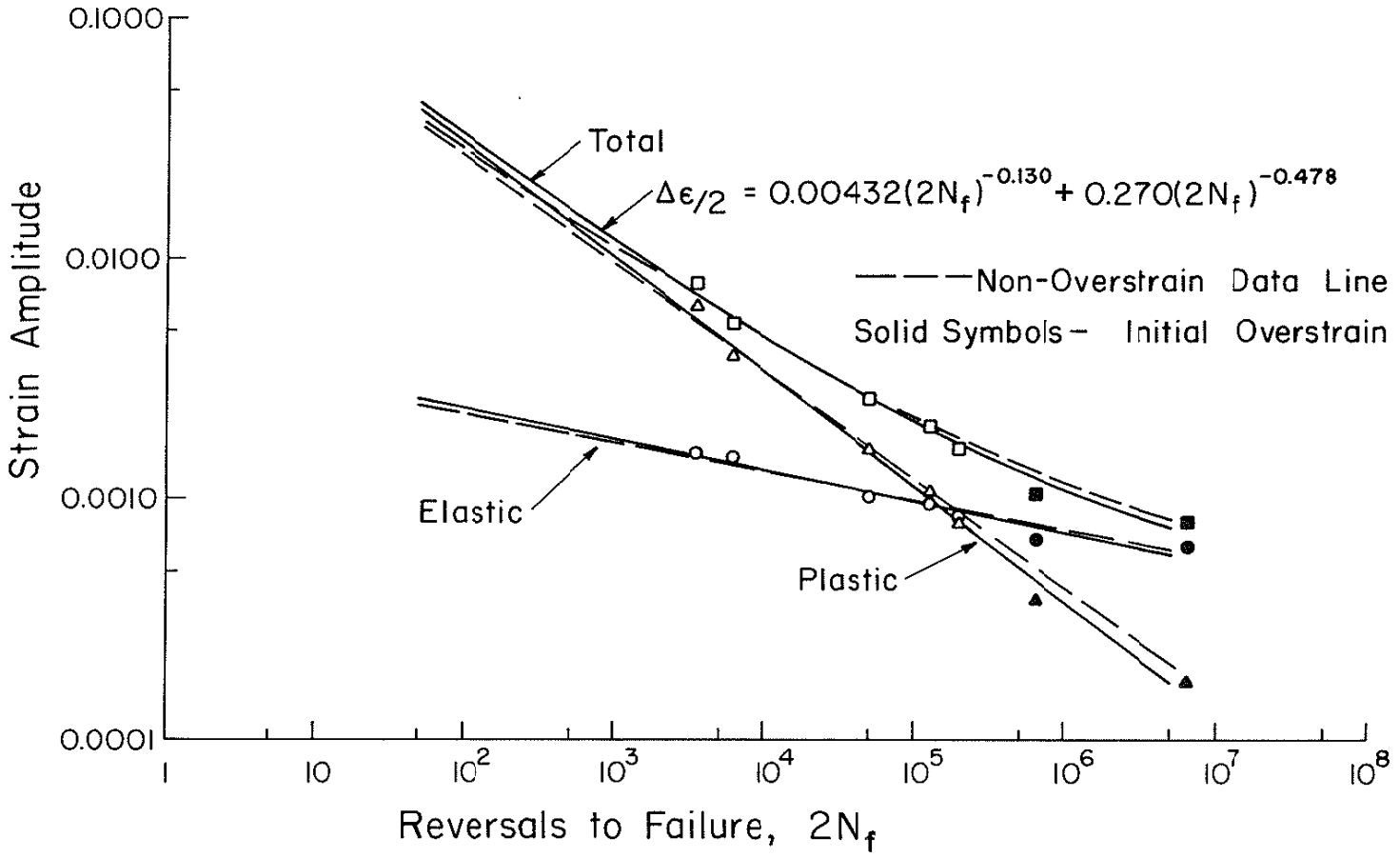

Fig. 36 Strain – Reversals to Failure Data for Sheet Steel Subjected to Initial Overstrains

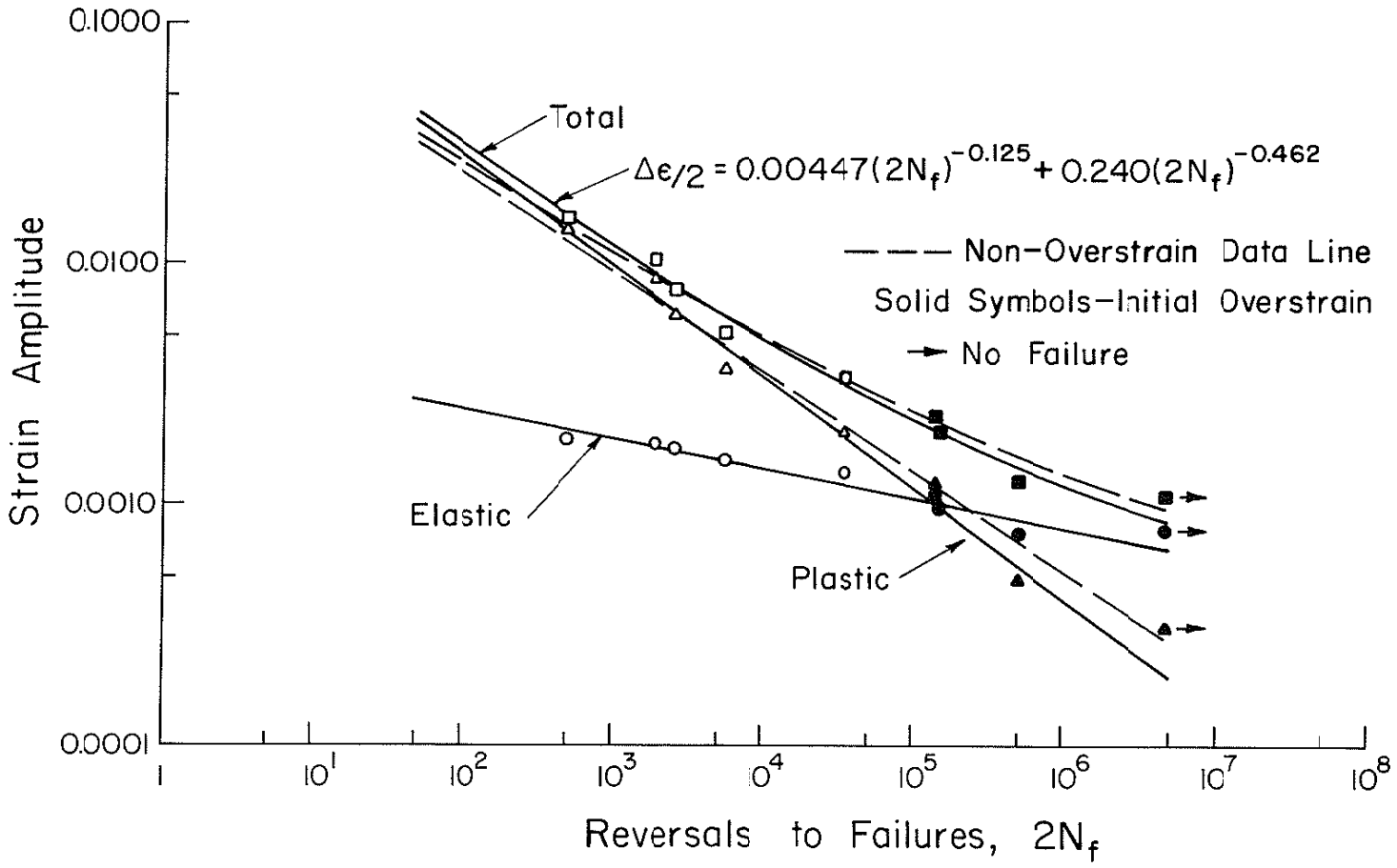

Fig. 37 Strain–Reversals to Failure Data for Bar Steel Subjected to Initial Cyclic Overstrains

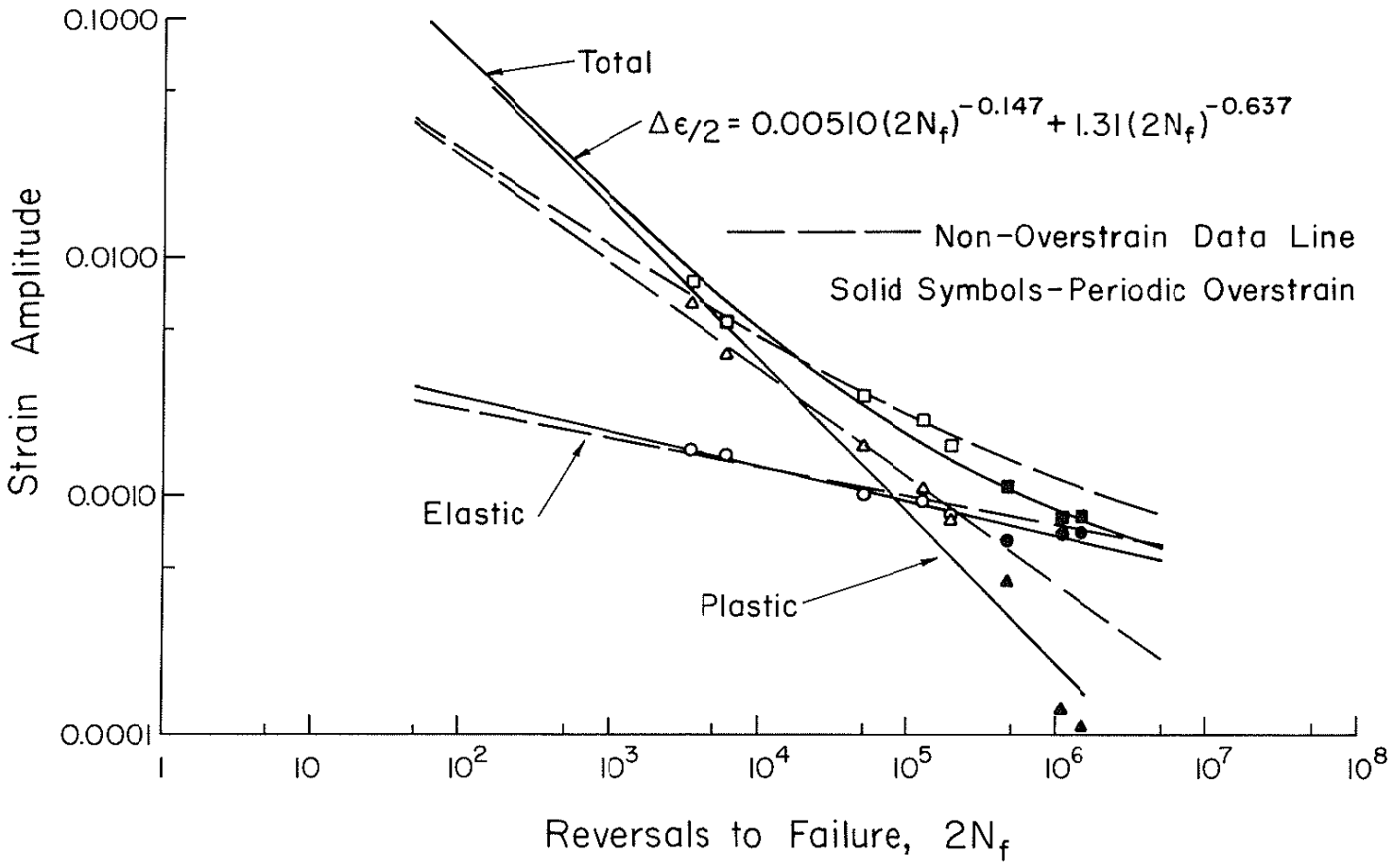

Fig. 38 Strain- Reversals to Failure Data for Sheet Steel Subjected to Periodic Cyclic Overstrains

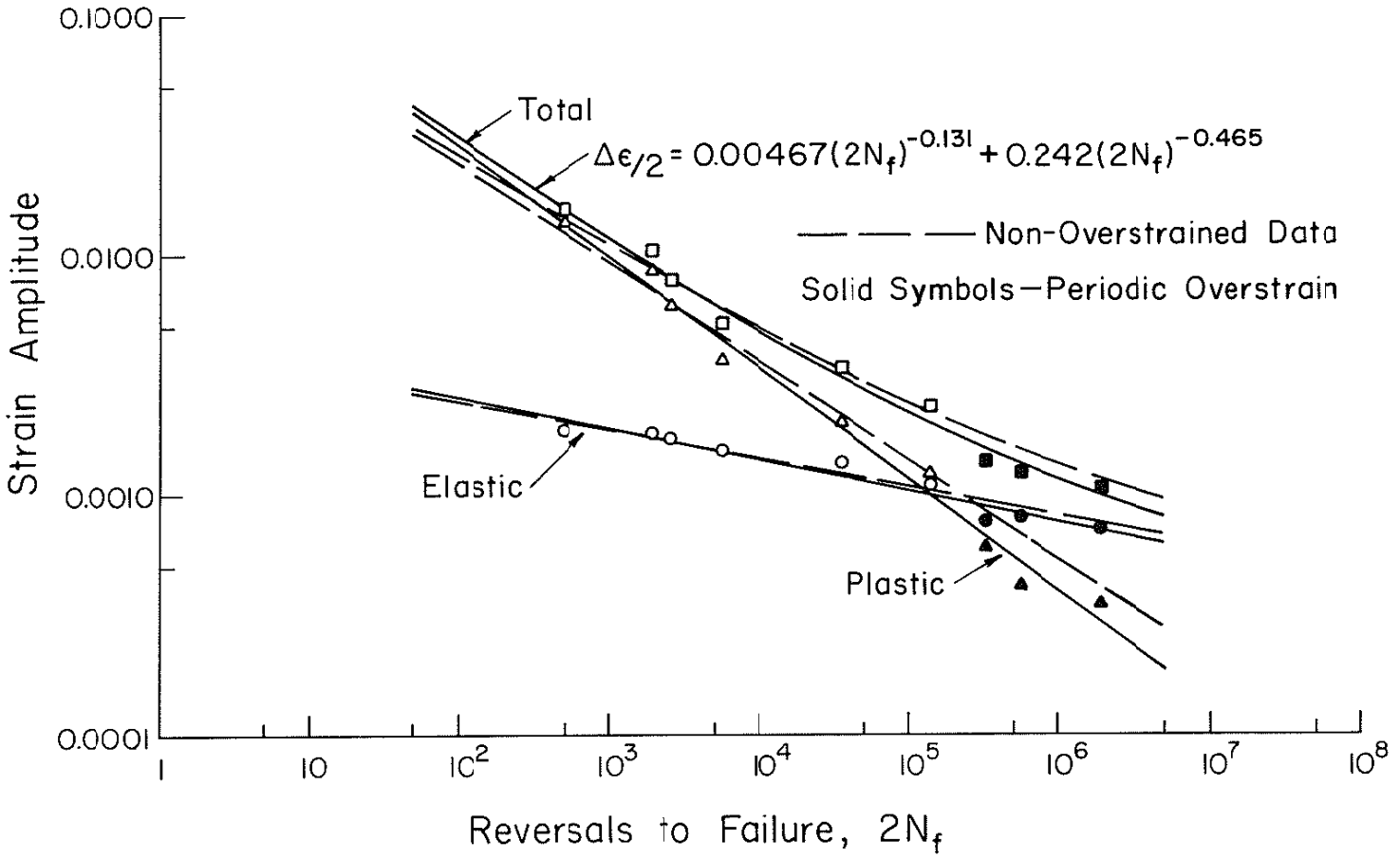

Fig. 39 Strain-Reversals to Failure Data for Bar Steel Subjected to Periodic Cyclic Overstrains

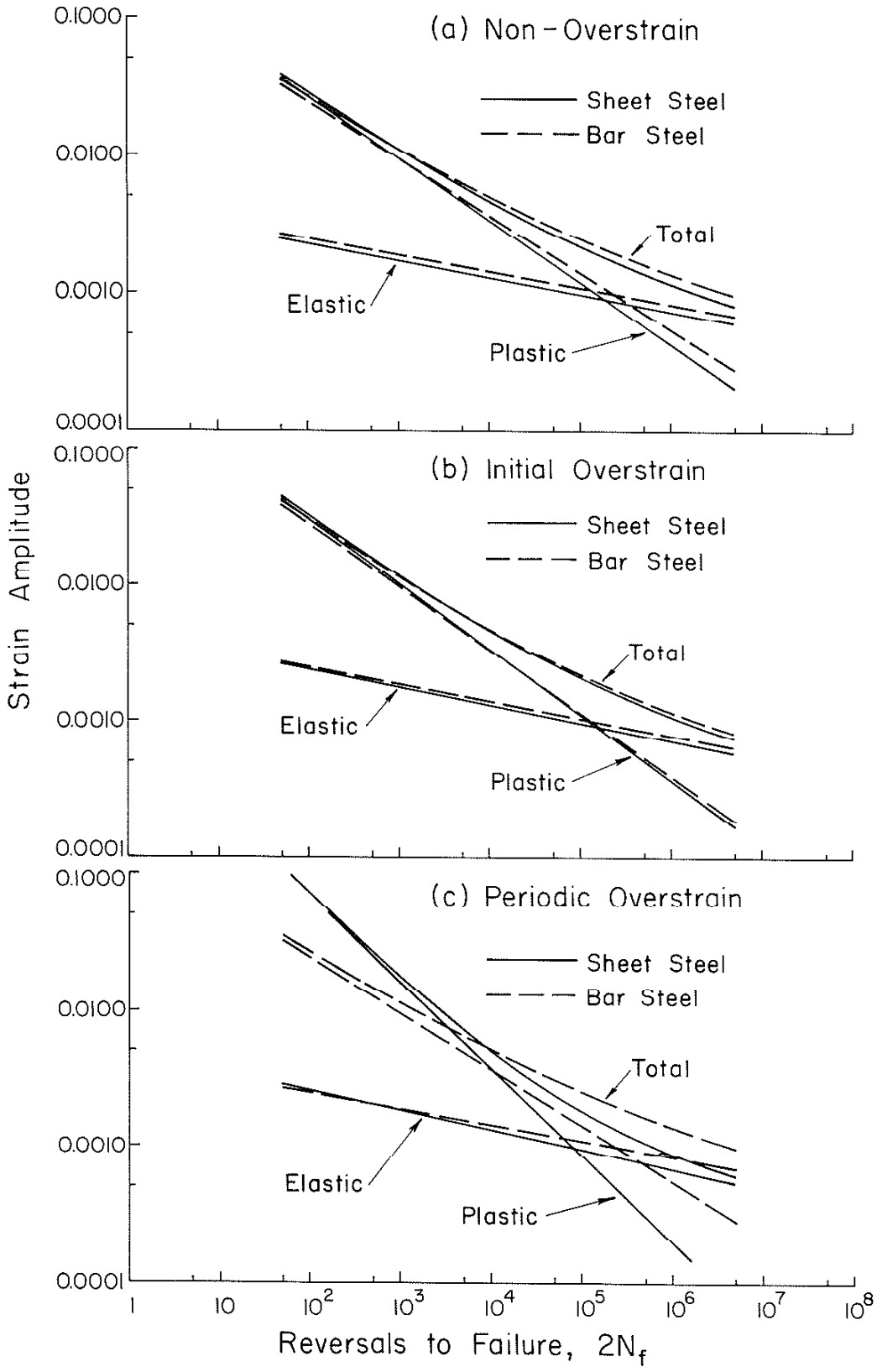

Fig. 40 Comparison of the Strain-Life Data for the Sheet and Bar Steels